

**Ing. Peter Kaľavský**

**Summary of the dissertation thesis**

**GPU-ACCELERATED MODEL-BASED MEASURING METHODS  
FOR INVESTIGATION OF CARDIAC ELECTRICAL ACTIVITY**

Submitted in fulfillment of the requirements  
for the degree of **Philosophiae Doctor, PhD.**

in doctoral study programme:  
**Measurement Technology**

in study field:  
**5.2.54 Measurement Technique**

Bratislava, August 2016

SLOVAK UNIVERSITY OF TECHNOLOGY IN BRATISLAVA  
FACULTY OF ELECTRICAL ENGINEERING AND INFORMATION TECHNOLOGY

**Ing. Peter Kaľavský**

**Summary of the dissertation thesis**

**GPU-ACCELERATED MODEL-BASED MEASURING METHODS  
FOR INVESTIGATION OF CARDIAC ELECTRICAL ACTIVITY**

Submitted in fulfillment of the requirements  
for the degree of **Philosophiae Doctor, PhD.**

in doctoral study programme:

**Measurement Technology**

Bratislava, August 2016

Proposed thesis was elaborated in the external form of study at the:

Institute of Measurement Science  
Slovak Academy of Sciences  
Dúbravská cesta 9, 841 01 Bratislava

Author: **Ing. Peter Kaľavský**  
Institute of Measurement Science  
Slovak Academy of Sciences  
Dúbravská cesta 9, 841 01 Bratislava

Supervisor: **doc. Ing. Milan Tyšler, CSc.**  
Institute of Measurement Science  
Slovak Academy of Sciences  
Dúbravská cesta 9, 841 01 Bratislava

Reviewers: **prof. Dr. György Kozmann, DSc.**  
Department of Electrical Engineering and Information Systems  
Faculty of Information Technology, University of Pannonia  
Egyetem utca 10, Veszprém 8200, Hungary

**RNDr. Vavrínek Szathmáry, CSc.**  
Dunajská 60, 811 08 Bratislava

Summary of the dissertation thesis was submitted on: 31.5.2016

Place of dissertation defense: Institute of Measurement Science (courtroom)  
Slovak Academy of Sciences,  
Dúbravská cesta 9, 841 04 Bratislava

Date and time of dissertation defense: **25th August 2016 from 11:30 a.m.**

**doc. Ing. Milan Tyšler, CSc.**  
Director of IMS SAS

## Abstrakt

Zlyhávanie srdca je stav, pri ktorom je v dôsledku rozličných faktorov poškodená schopnosť srdca pumpovať krv do ľudského tela. Jedným z týchto faktorov sú abnormality vo vedení elektrických impulzov v srdci. Keďže existuje veľké množstvo možných abnormalít, na ich preskúmanie sa často používajú matematické modely. Najvyspelejšie modely na simulovanie elektrickej aktivity srdca a elektrokardiogramov (EKG) sú reakčno-difúzne (R-D) modely. Výpočtová náročnosť R-D modelov je však taká vysoká, že simulácia čo i len jedného úderu srdca trvá hodiny aj na výkonnom superpočítači. Aby bolo možné využiť matematické modely srdca i v klinickej praxi je dôležité výrazne redukovať výpočtové časy simulácií.

V predloženej práci je predstavený možný koncept urýchlenia simulácii elektrickej aktivity srdca. Bol navrhnutý výpočtovo rýchly plne anizotropický model priamej úlohy elektrokardiografie na simulácie aktivačnej sekvencie v srdci a na výpočet EKG. Model bol implementovaný v paralelnom programovacom jazyku CUDA a podporuje masívne paralelné výpočty na grafických procesoroch (GPU). Šírenie elektrickej aktivácie v srdci bolo modelované použitím eikonalovej rovnice. Eikonalová rovnica umožňuje vypočítať aktivačnú sekvenciu, respektíve časy, v ktorých excitačný front prechádza cez jednotlivé body myokardu. Pohyb excitačného frontu možno sledovať použitím priestorového rozlíšenia, ktoré je o jeden rád menšie ako je rozlíšenie R-D modelu, ktoré je potrebné na rekonštrukciu strmého skoku akčného potenciálu, výsledkom čoho sú mnohonásobne kratšie výpočtové časy a mnohonásobne menšie požiadavky na kapacitu pamätí výpočtových systémov. Aktivačné časy vygenerované použitím eikonalovej rovnice spoločne s predefinovanými akčnými potenciálmi a prenosovou funkciou nazývanou „zvodové pole“ boli následne použité na simulovanie povrchových EKG. Výpočtová rýchlosť navrhnutého modelu bola otestovaná na štyroch realistických patientskych geometriách s rozlíšením 1 mm za použitia dvoch výkonnostne rozdielnych GPU. Výsledky ukázali, že model dokáže simulovať aktivačnú sekvenciu a štandardné 12-zvodové EKG na profesionálnom GPU v priebehu 3 sekúnd. Simulované aktivačné časy a EKG boli porovnané s hodnotami získanými z R-D modelu. Aktivačné sekvencie vypočítané oboma modelmi vykazovali po vizuálnej stránke podobné charakteristiky šírenia. Absolútna chyba aktivačných časov v približne 270 000 porovnávaných bodoch kolísala lokálne od 0 až do 30.08 ms, avšak v 94% bodov nepresiahla 10 ms. Simulované EKG boli porovnané individuálne pre každý z dvanástich zvodov. Akceptovateľné rozdiely boli dosiahnuté len pri porovnávaní QRS komplexov, pre ktoré bola vyhodnotená priemerná RMS relatívna odchýlka rovná 0.51 a priemerný korelačný koeficient rovný 85.05%. Po vizuálnej stránke sa väčšina QRS komplexov zhodovala tvarom, polaritou a trvaním a vykazovala rozdiel približne 0.3 mV v amplitúde vrcholu R vlny. Porovnanie repolarizačných častí EKG kriviek ukázalo mnoho rozdielov, a to aj napriek tomu, že navrhnutý model uvažuje s transmúrálou heterogenitou trvania akčných potenciálov. Aby bolo možné urobiť rozumné závery ohľadom reprodukcie T vlny, je potrebné vykonať hlbšiu štúdiu používaných parametrov a porovnať simulované a merané EKG krivky. Praktická užitočnosť modelu bola otestovaná na optimalizačnej procedúre. Jej cieľom bolo nájsť čo najlepšiu zhodu medzi simulovanými a meranými aktivačnými časmi, a to postupnou úpravou polôh jedného stimulačného bodu a hodnôt regionálnych rýchlostí vedenia vzruchu. Vďaka výpočtovej rýchlosti modelu bola v priebehu niekoľkých minút detegovaná skupina parametrov, vedúca ku korelačným koeficientom medzi simulovanými a meranými aktivačnými časmi v rozsahu od 85 do 94%.

Navrhnutý model je ako súčasť inverzných procedúr aktívne využívaný na Ústave výpočtových vied v Lugane. Výstupy z inverzných procedúr slúžia ako počiatočný odhad pre nastavenie parametrov R-D modelu, pomocou ktorého sa realizuje finálne ladenie zhody medzi simulovanými a meranými dátami. Dlhodobým cieľom je vyvinúť technológie, ktoré by zlepšili diagnostiku abnormalít elektrickej aktivácie srdcových komôr.

## Contents

<b>Abstrakt</b> .....	<b>i</b>
<b>1 Introduction</b> .....	<b>1</b>
<b>2 Goals of the dissertation thesis</b> .....	<b>2</b>
<b>3 Whole-heart models</b> .....	<b>3</b>
3.1 Bidomain and monodomain model .....	3
3.2 Eikonal model .....	4
<b>4 General-purpose computing on graphics processing units</b> .....	<b>5</b>
<b>5 Proposed heart model anatomy</b> .....	<b>5</b>
5.1 Mapping of the cell type code to a substance.....	6
5.2 Mapping of the cell type code to an action potential .....	7
5.3 Implementation of the ventricular anisotropy .....	7
5.4 Summary of model parameters .....	9
<b>6 Numerical implementation of the eikonal equation</b> .....	<b>9</b>
6.1 The finite-element discretization.....	10
6.2 The data structures .....	11
6.3 Jacobi iterative method .....	11
6.4 Fast iterative method .....	12
<b>7 Numerical implementation of the ECG computation</b> .....	<b>12</b>
7.1 The data structures .....	13
7.2 Simple method .....	13
7.3 Fast method.....	14
<b>8 Results and discussion</b> .....	<b>14</b>
8.1 Real-time multichannel ECG signal processing on GPU.....	15
8.2 Forward modeling results.....	16
8.2.1 Comparison of eikonal solver runtimes .....	17
8.2.2 Comparison of ECG solver runtimes.....	18
8.2.3 Comparison of activation times computed by Propag and Propeiko .....	20
8.2.4 Comparison of ECGs computed by Propag and Propeiko .....	21
8.3 Matching of simulated and measured activation times .....	24
<b>9 Conclusion</b> .....	<b>25</b>
9.1 Contributions of the thesis .....	26
<b>Bibliography</b> .....	<b>27</b>
<b>List of author's publications</b> .....	<b>29</b>

## 1 Introduction

Heart failure is a condition in which the heart muscle cannot pump enough blood to fulfill the needs of other organs in the body. It is one of the most common diseases in the western world [1]. Heart failure may be caused by many factors, one of which are abnormalities in the conduction of electrical impulses through the heart. These abnormalities may change the normal activation of individual heart regions, and hence influence the overall heart contraction. Studies published in the last few years are suggesting that there is a large variety in these abnormalities, and that a better characterization of individual factors is important for an appropriate choice of treatment.

Nowadays, thanks to an enormous computational power of parallel hardware resources and advances in numerical methods, it is common to study complex biological systems by the use of mathematical models and computer simulations. Models enable to test various hypotheses and predict the behavior of evaluated systems by simple tuning of their parameters. The outputs of the simulations may be compared with measured data, so the conclusions about the hypotheses can be drawn. The current state of the art model for forward simulation of cardiac electrical activity is so called bidomain model [2], [3]. The bidomain model assumes the cardiac tissue consisting of interleaving intracellular and extracellular domains that are separated by a cell membrane with ionic channels. The prominent feature of this model is its ability to account for different anisotropic electrical conductivities in both domains. The bidomain model allows for the simulation of cardiac extracellular potentials, transmembrane potentials (and hence also activation times) and when coupled with the torso, to simulate the electric field within the body and on the body surface as well. The outputs of the model can be compared with invasively measured endocardial or epicardial potentials or activation times, and also with noninvasively measured body surface ECGs. One such a highly realistic computer model of the human heart [3], [4] tailored to the individual patient's anatomy and physiology characteristics is routinely used at the Institute of Computational Science in Lugano. The group around Prof. Mark Potse tries to optimize the match between measured and simulated activation times and ECGs by feeding the input parameters of the model with various physiological and pathological quantities. With this method very good matches can be obtained, and it is considered to be a very promising approach to identify tissue abnormalities that could not be diagnosed in any other way [5]. However, due to its computational complexity the model has to run on a large supercomputer and the solution for a single heart beat takes in the order of hours (eventually in the orders of tens of minutes if the simplified monodomain variant is used to simulate the electrical propagation). Hence in total it usually takes several weeks to adapt the model to a single patient. The goal of this thesis is therefore to develop a computationally fast forward model that could significantly speed up and automate the initial tuning of model parameters.

In general, computationally fast models simulating the electrical activity of the heart are based on simplified formulation of cardiac sources and volume conductor, what allows them to achieve high execution speed at the expense of accuracy. Many of them assume isotropic conductivity of the heart and torso regions and rely on simple shape geometries. However, in this study we proposed a forward model that is much more complex and realistic than those in the existing approaches. In particular, it takes into account the anisotropic nature of the cardiac tissue as well as the anisotropy and heterogeneity of the human torso and in addition is tailored to patient-specific geometries. The proposed model simulates the spread of excitation within the heart by the use of the eikonal formulation [6], [7] the output of which is set of activation times. These activation times together with precomputed action potentials and a transfer function known historically as "lead field" [8], [9] are subsequently used to simulate surface ECGs. Eikonal approach instead of solving for

transmembrane potentials, computes only the activation sequence or the times at which the excitation wavefront passes through a given points in the myocardium. From the computational point of view it is important that the motion of the wavefront is observed at the scale of the order of 1 mm that is much larger than the 0.1 - 0.2 mm scale required to reliably reconstruct the sharp upstroke of the action potential by the R-D models (bidomain or monodomain). As a result much shorter computation times can be reached. The spatial discretization at a resolution of 1 mm is high enough to resolve the local fiber orientation and an anisotropic computation of the dipole sources, thus the model is able to account for the influence of anisotropic conductivity on the ECG, as well as on the propagation velocity. When compared to R-D models the only important simplification is that the influence of ionic heterogeneity on the propagation velocity and repolarization characteristics is neglected.

For practical applicability it is crucial that the computer models are fast enough and preferably that they can soon work on local computers rather than remote supercomputers. To achieve this, the proposed model supports massively parallel computation on graphic processing units (GPUs). The GPUs were originally designed for the processing of complex computer graphics. However, over the years they evolved into massively parallel devices with thousands of execution units called cores and nowadays they are commonly used in the high performance computing (HPC) sector for performing non-graphical, so called general-purpose computations [10]. Today's most powerful high-end GPUs are reaching more than 5 TFLOPS (tera floating-point operations per second) of double precision floating point performance. Each GPU core is much simpler and less powerful than a core of central processing unit (CPU), however, hundreds or thousands of these modest cores on a single chip outperform a CPU by two orders of magnitude. Nevertheless, GPUs are accelerators specialized exclusively for processing of tasks that exhibit massive data parallelism, thus the tasks solving of which requires to execute the same instruction on a big data set in parallel. Proposed model consisting of hundred of thousands computational elements indeed hides enormous potential for data parallelization.

To conclude, the goal of this thesis is to develop a GPU-accelerated fully anisotropic forward model for the investigation of cardiac electrical activity that due to its computational efficiency could be effectively used as part of inverse models to estimate the patient-specific parameters and to make patient-specific predictions of cardiac activation patterns and ECGs.

## **2 Goals of the dissertation thesis**

As mentioned above, the main goal of this thesis is to develop a GPU-accelerated fully anisotropic forward model for the simulation of the activation sequence in the cardiac tissue and the computation of ECGs. Primary attention will be focused on the implementation details of parallel algorithms running on GPUs. In particular, the aims are:

- to investigate possible utilization of general-purpose computations on GPUs for processing of multichannel ECGs and primary for solving the forward problem of electrocardiography;
- to develop fully anisotropic model for solving the forward problem of electrocardiography. The forward model is aimed at the simulation of the activation sequence in the cardiac tissue using the eikonal equation and at the simulation of the ECGs using three main components: the activation sequence obtained from the eikonal equation, precomputed action potential and the transfer function known as the lead field;
- to implement the forward model on a massively parallel CUDA GPU;

- to evaluate the parallel computational methods embedded in the proposed forward model in terms of their speedup and parallel scalability on different GPUs and to compare the resulting simulated activation sequences and ECGs with the results obtained from a R-D model as a reference.

### 3 Whole-heart models

Over the past few decades a tens of models simulating electrophysiological behavior of the human heart with different levels of details have been introduced. In the following section first, the state-of-the-art model for the simulation of electrical activity of the heart so called bidomain model together with it simplified variant called monodomain model will be introduced, and consequently computationally faster more approximate eikonal model will be discussed.

#### 3.1 Bidomain and monodomain model

In the bidomain approach [11], [2] the myocardium is represented by two interpenetrating domains, one for the intracellular (subscript  $i$ ) and the other for the extracellular region (subscript  $e$ ) of the cardiac tissue. The key aspect of the model is that both these domains are assumed as coexisting at all points in the myocardium. The connection between the two domains is realized through the cell membrane, which contains the ionic channels represented by voltage and time dependent currents that generate action potentials within the cells. Bidomain equations are given in the following form

$$\nabla \cdot [(\mathbf{G}_i + \mathbf{G}_e)\nabla\Phi_e] = -\nabla \cdot (\mathbf{G}_i\nabla V_m) + I_{s1} \quad (3.1)$$

$$\nabla \cdot (\mathbf{G}_i\nabla V_m) + \nabla \cdot (\mathbf{G}_i\nabla\Phi_e) = \beta \left( C_m \frac{\partial V_m}{\partial t} + I_{ion} \right) - I_{s2} \quad (3.2)$$

where  $\mathbf{G}_i$  and  $\mathbf{G}_e$  ( $\text{Sm}^{-1}$ ) are the intracellular and extracellular conductivity tensors,  $\Phi_e$  (V) is the electric potential in the extracellular domain,  $V_m$  (V) is the transmembrane potential,  $\beta$  ( $\text{m}^{-1}$ ) is the surface to volume ratio of the cell membrane  $I_{ion}$  ( $\text{Am}^{-2}$ ) is the ionic current density per unit area, and finally the  $I_{s1}$  and  $I_{s2}$  (A) are external stimulus current applied to extracellular and intracellular domain, respectively. The Equation (3.1) describes the conservation of current and by providing a transmembrane potential distribution it is used to solve the extracellular potential. The Equation (3.2) describes the flow of current through the cellular membrane and serves to calculate the transmembrane potential distribution [3], [12].

If the intracellular and extracellular conductivity tensors  $\mathbf{G}_i$  and  $\mathbf{G}_e$  are proportional,  $\mathbf{G}_e = \lambda\mathbf{G}_i$ , with  $\lambda$  be a constant scalar factor, or in other words, if the two media have the same anisotropy ratio, then the system of bidomain equations (3.1) and (3.2) can be reduced to a monodomain R-D equation

$$\nabla \cdot (\mathbf{G}\nabla V_m) = \beta \left( C_m \frac{\partial V_m}{\partial t} + I_{ion} \right) - I_s \quad (3.3)$$

where  $\mathbf{G}$  is a tensor of effective conductivities. The extracellular potential  $\Phi_e$  plays no role in monodomain equation (3.3), hence the  $V_m$  can be computed independently from  $\Phi_e$ , what substantially reduces the computational complexity of the monodomain model comparing with the bidomain model.

### 3.2 Eikonal model

The eikonal model takes into account only the depolarization phase of the cardiac excitation process and approximates the thin depolarization region by propagating excitation wavefront. The output of the eikonal model is set of activation times at which the wavefront passes through the myocardium. A governing equation for the activation time is an eikonal equation. Colli-Franzone et al. in [6], derived the eikonal equation from the bidomain equations applying a perturbation technique, hence both approaches can be compared. The derivation is based on relating the velocity of the excitation wavefront to the anisotropic conductivities of the intracellular and extracellular domains. The eikonal model proposed in this thesis is based on the zero-order eikonal equation given by

$$\begin{cases} \rho(x)\sqrt{\mathbf{G}(x)\nabla\Psi(x) \cdot \nabla\Psi(x)} = 1, & x \in \Omega \setminus \{x_i\}, \\ \Psi(x_i) = t_i, & i = 1, \dots, N. \end{cases} \quad (3.4)$$

where  $\Psi$  (ms) is the activation time,  $\mathbf{G}$  ( $\text{mS cm}^{-1}$ ) is the tensor of effective conductivities defining the local anisotropy of the tissue,  $\rho$  ( $(\text{cm}^3/(\text{ms}^2\text{mS}))^{1/2}$ ) is a membrane parameter, and  $N$  is the number of early activation sites. The early activation site represents a point source  $x_i$  with initial time  $t_i$  from which the excitation front initiates (see Figure 3.1).

The membrane parameter  $\rho$  enables to match the conduction velocity  $\theta$  ( $\text{cm ms}^{-1}$ ) of the eikonal equation to the one from the bidomain equations. The eikonal model approximates the conduction velocity along the given direction  $k$  as

$$\theta_k = \rho\sqrt{\sigma_k} \quad (3.5)$$

where  $\sigma_k$  represents an effective conductivity, while the corresponding conduction velocity in the bidomain approach is expressed as

$$\theta_k = \alpha \sqrt{\frac{\sigma_k}{\beta}} \quad (3.6)$$

where  $\beta$  ( $\text{cm}^{-1}$ ) is the surface to volume ratio of the cell membrane and  $\alpha$  ( $\text{cm}/(\text{ms mS}^{-1/2})$ ) is scaling factor that links the ionic model and conduction velocity. Combining (3.5) and (3.6) we obtain the expression for the membrane parameter  $\rho$  that can be used to link the eikonal and bidomain parameters

$$\rho = \frac{\alpha}{\sqrt{\beta}} \quad (3.7)$$

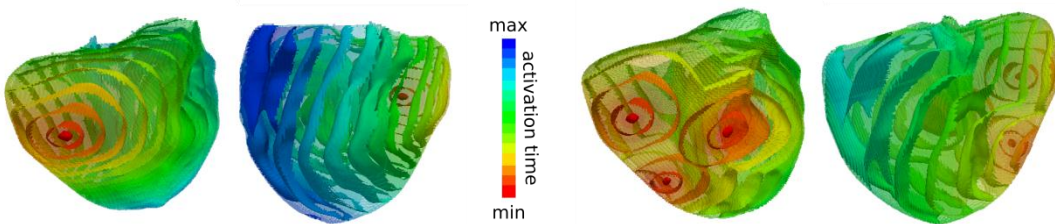


Figure 3.1: The isosurfaces of ventricular activation times. Early activation sites (single on the left side and three on the right side) are shown as small red spheres.

## 4 General-purpose computing on graphics processing units

The algorithms designed in this work are destined for the GPUs based on CUDA architecture (Compute Unified Device architecture). CUDA is parallel hardware and software platform developed by Nvidia. The enormous computational power of CUDA GPUs lies in the massive parallelism. In CUDA execution model millions of running threads are organized into the groups of 32 consecutive threads called warps [10], [13] that are mapped among available cores. When a warp idles due to arithmetic or memory instruction latencies (10 – 20 and 400 – 800 cycles latencies, respectively [14]), the warp scheduler immediately selects another warp for the execution. Here lies the power and effectiveness of the GPUs. Massive number of available warps (or threads) ready for execution hides long lasting latencies and permanently utilizes the GPU resources.

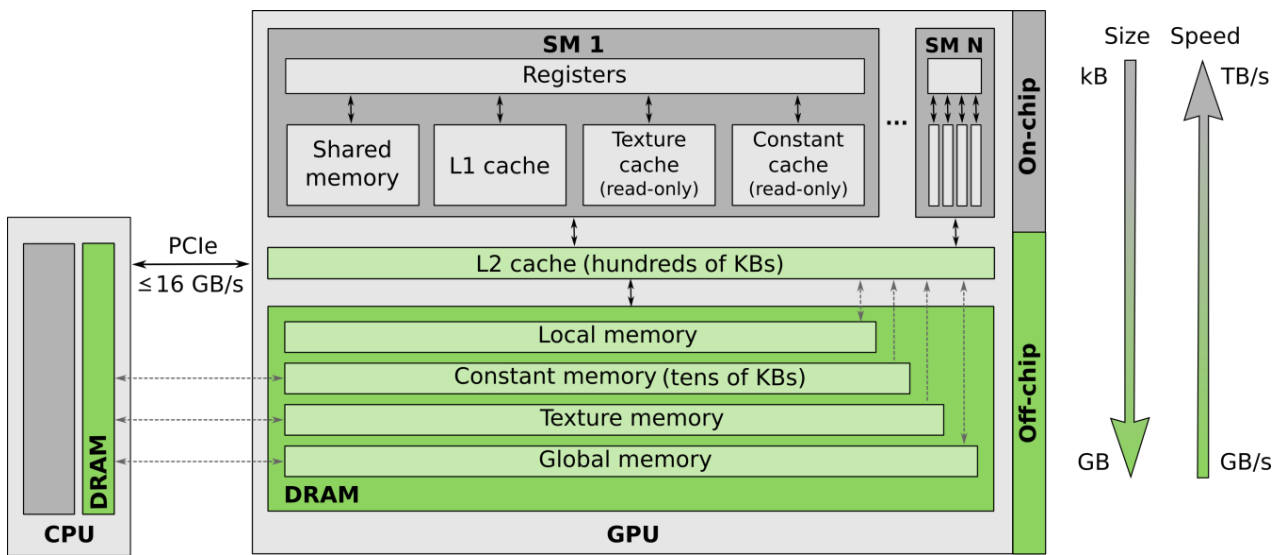


Figure 4.1: CUDA memories.

The key impact on the GPU application performance has a proper management of the various types of GPU memories. The peak GPU performance can be achieved when the fast but lower capacity on-chip memories are heavily utilized with minimal communication with the slower but higher capacity off-chip memories. In addition, to maximize the use of bytes that travel through the bus it is necessary to keep data in memories aligned and access them in coalesced manner. Coalesced memory accesses are especially important when accessing the global memory, in which the majority of data transfers starts and terminates. In general it is important to let the consecutive threads to access the data in consecutive memory locations. If strided memory access are required, instead of single chunk of data fetched from memory, several chunks are fetched and the memory bandwidth is significantly wasted [13], [15].

## 5 Proposed heart model anatomy

Proposed heart model uses a structured cubic mesh. A basic building element of the model is a cubic element called voxel (Figure 5.1). The corners of a voxel are called vertices. The model anatomy is defined inside a file that contains a cell type code (one byte value) for each voxel of the model. The cell type code determines

what material properties are associated with a voxel. Material properties are defined by six conductivities, three for the intracellular domain  $\sigma_{il}$ ,  $\sigma_{it}$ ,  $\sigma_{ic}$  and three for the extracellular domain  $\sigma_{el}$ ,  $\sigma_{et}$ ,  $\sigma_{ec}$ , and by the square power of the membrane parameter  $\rho$ . If the comparison with the R-D model is of interest, surface to volume ratio  $\beta$ , and scaling factor  $\alpha$  (see (3.7)). can be used instead of  $\rho$ . Once the material properties are mapped to a voxel, a voxel becomes a cube. The corners of a cube are called nodes. In the patient-specific geometries that were used in our experiments on around 10 % of voxels and vertices acted as cubes and nodes, respectively). The model works by default with the resolution  $h = 1$  mm, however  $h$  is a parameter that can be changed in each spatial direction.

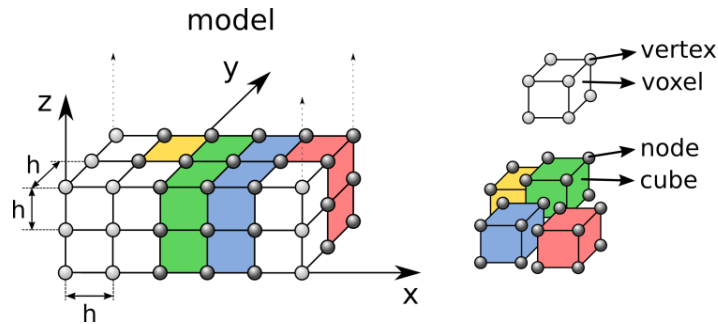


Figure 5.1: Basic building elements of the proposed heart model.

## 5.1 Mapping of the cell type code to a substance

The default arrangement of the cell type code data of our realistic heart models forms a continuous layered structure of substances. In Figure 5.2 this layered structure across the transverse and longitudinal section of the right and left ventricles can be seen.

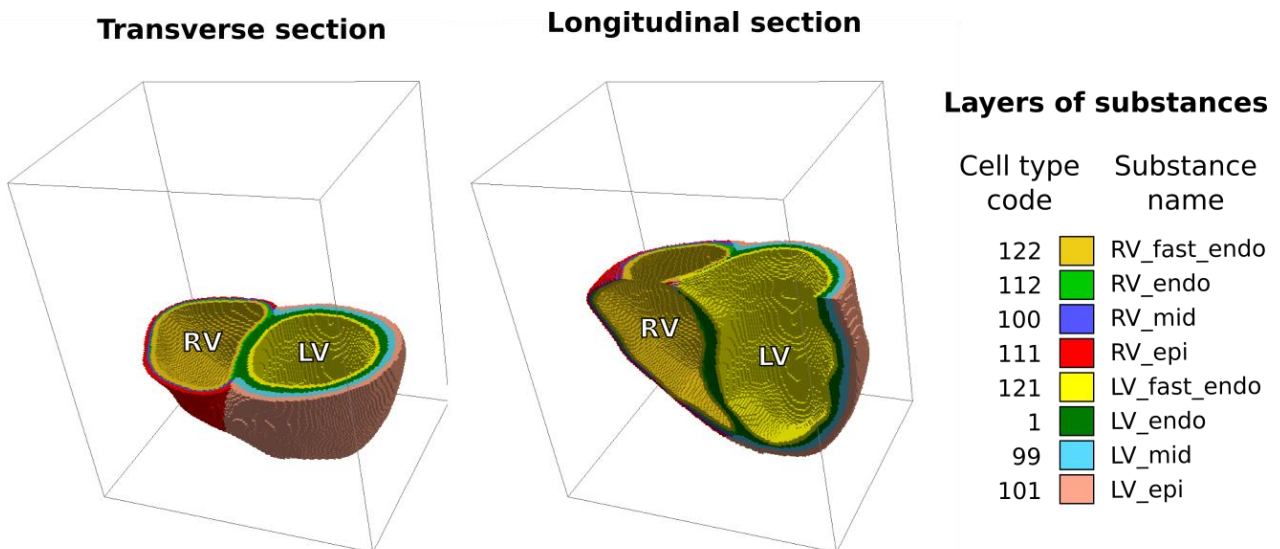


Figure 5.2: A layered structure of the substances across the transverse and longitudinal section of the right (RV) and left (LV) heart ventricles of a realistic geometry. Only layers with specified substances are displayed.

The branches of the His bundle and the system of Purkinje fibers were in the proposed model roughly approximated by a thin subendocardial layers (yellow layers in Figure 5.2). We called this thin layers "fast endocardial layers". The purpose of these fast endocardial layers is to rapidly spread the excitation through the ventricles. On the one hand, this approach significantly simplifies the reality, but on the other hand, it allows a simple and quite accurate control of the initialization of the cardiac activation, which is a fundamental prerequisite for correct simulation of ECGs [16].

## 5.2 Mapping of the cell type code to an action potential

In order to take into account also the action potential heterogeneity across the heart, the model determines the mapping of the cell type codes to the predefined action potentials. However, the action potentials are mapped to the vertices, instead of voxels of the model. In our simulations, the cell heterogeneity was only considered as a transmural variation of the action potential duration (APD) in both ventricles. Hence, we assumed that the epicardial cells have the shortest APD, the endocardial cells have an intermediate APD and the M cells the longest APD. In addition, we assumed that the epicardial and mid-myocardial APDs were a bit shorter in the right ventricle than in the left ventricle. The action potential waveforms used in our simulations are depicted in Figure 5.3. These waveforms were generated by the Ten Tusscher-Noble-Noble-Panfilov (TNNP) membrane model [17] and Ten Tusscher-Panfilov (TP06) membrane model [18].

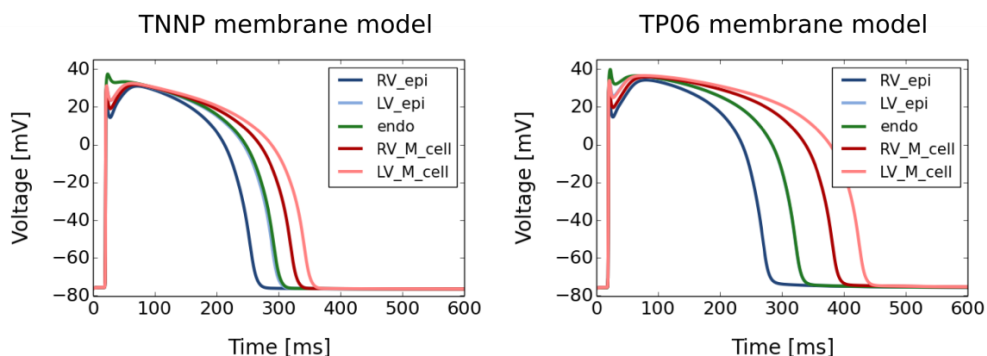


Figure 5.3: The action potentials waveforms used for the simulation of ECGs (in both graphs the waveform marked as endo overlaps with the waveform marked as LV\_epi).

## 5.3 Implementation of the ventricular anisotropy

The cardiac tissue is arranged anisotropically. The anisotropy of cardiac tissue is one of the main factors affecting the propagation of electrical waves and contraction in ventricles of the heart [19]. Experimental measurements [20] showed that the fastest propagation is along the myocardial fibers and is 2 - 4 times faster than propagation across the fibers [21].

Measurements of human left ventricular tissue made by Streeter [22] showed a continuous transmural rotation of the helix angle  $\alpha$ , which is the angle between the fiber direction and the atrioventricular ring direction in a plane parallel to the local endocardial surface (see Figure 5.4). If the orientation from base to

apex is chosen to be  $\pm 90^\circ$ , and the angle  $0^\circ$  represents the equatorial direction, then  $\alpha$  changes from  $+55^\circ$  in the subendocardium to  $-75^\circ$  in the subepicardium.

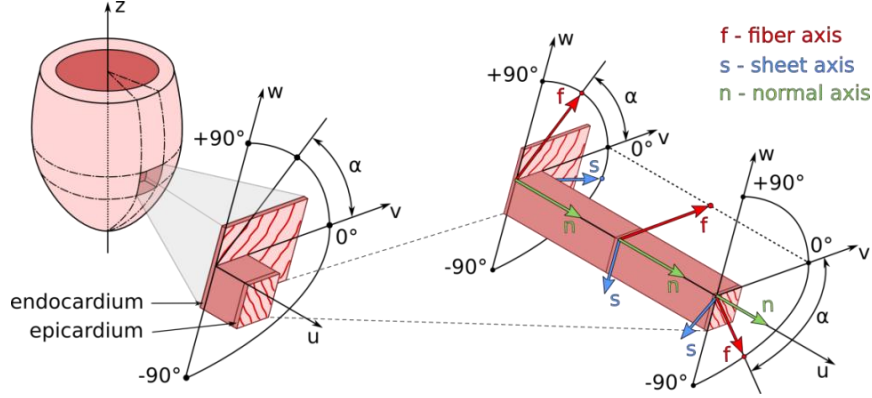


Figure 5.4: The Streeter's definition of transmurally rotating helix angle  $\alpha$  (top left). The helix angle is evaluated on a block of cardiac tissue cutout transmurally from the left ventricular wall. (Adapted by author from [23].)

For modeling purposes, it is convenient to define a natural set of material directions to characterize the structure of myocardial tissue at an arbitrary point in the heart wall. Typically three unit vectors are used: unit vector directed along the fibers  $\mathbf{f}$ , unit vector perpendicular to the fibers in the sheet plane  $\mathbf{s}$  and unit vector normal to the sheet plane  $\mathbf{n}$  (the detailed studies of LeGrice et al. [20], [24] shown that the fibers in the heart are locally organized into laminar structures called sheets).

To account for the anisotropic properties of the ventricular tissue the proposed model utilizes three angles  $\varphi$ ,  $\gamma$ , and  $\alpha$  to describe the above mentioned fiber, sheet, and normal orientations. These three angles relate to the Euler angles [25], and are used to express the fiber orientation in local material coordinate system with respect to a fixed coordinate system.

For the determination of the myocardial fibers the rule-based approach was used [3]. First, for each ventricular node, a minimal distance to the endocardial  $d_{endo}$  and epicardial  $d_{epi}$  surface was computed. Afterwards, for each node of the mesh a thickness parameter  $e$  was evaluated using

$$e = \frac{d_{epi}}{d_{endo} + d_{epi}} \quad (5.1)$$

and hence,  $e$  was equal to zero at the epicardium and one at the endocardium. Consequently, at each node of our mesh an average value  $\bar{e}$  was computed using the value of  $e$  at that node and the values of  $e$  at its 26 neighbors. In the next step the negative gradient of  $\bar{e}$ , thus a vector  $\mathbf{n} = -\nabla\bar{e}$ , was determined. The vector  $\mathbf{n}$  represented the unit vector in the direction normal to the sheet. One can imagine the sheets in the model as the "onion layers", with  $\mathbf{n}$  pointing from endocardium to epicardium. The unit vectors in the fiber direction  $\mathbf{f}$  were set orthogonal to the vectors  $\mathbf{n}$ , while taking into account a helix angle  $\alpha$  expressed as

$$\alpha = R(1 - 2\bar{e})^3 \quad (5.2)$$

where  $R$  was set equal to  $\pi/3$  for the left ventricle and  $\pi/4$  for the right ventricle.

## 5.4 Summary of model parameters

Relevant parameters of the proposed model are summarized in Table 5.1. The majority of them were already discussed in previous chapters. Two remaining, namely the early activation site, and the lead field are discussed here.

The early activation site (EAS) represents a stimulation site from which the electrical activation starts to propagate through the ventricles. EAS is defined by three coordinates  $x$ ,  $y$  and  $z$  that describe its position in the ventricles and by time constant  $t$  that represents the starting time of propagation (or delay of stimulation). The model enables to define several EASs for single activation.

The lead field ( $Z$ ) is used during the computation of ECG. Proposed model keeps precomputed values of  $Z$  for each of the simulated ECG leads. The computation of  $Z$  itself takes into account particular heart and torso anatomy and is described in Chapter 7. The lead field, in contrast to the cell type code data, and the three angles ( $\varphi$ ,  $\gamma$ , and  $\alpha$ ) describing the fiber and sheet orientations, is defined for each vertex of the model and is stored in a dedicated file.

mesh resolution $h$ (x, y, and z dimension)
parameter handling cell type codes
parameters handling precomputed angles encoding fiber architecture ( $\varphi$ , $\gamma$ , $\alpha$ )
square root of membrane parameter $\rho$
surface to volume ratio of cell membrane $\beta$
scaling factor $\alpha$ that links ionic model and conduction velocity
six conductivities ( $\sigma_{ib}$ , $\sigma_{ib}$ , $\sigma_{ic}$ , $\sigma_{eb}$ , $\sigma_{eb}$ , $\sigma_{ec}$ )
parameter <i>smap</i> for mapping of substances
parameter <i>imap</i> for mapping of action potentials waveforms
parameter defining three coordinates of early activation site and a time delay of stimulation
parameter handling precomputed action potential waveforms
parameter handling precomputed lead fields
parameters defining the length and resolution of simulated ECG

Table 5.1: Relevant parameters of proposed forward model.

## 6 Numerical implementation of the eikonal equation

Under suitable hypothesis on the coefficients and the initial data, there exists a unique closed-form viscosity solution [26] of the eikonal equation (3.4), which reads as follows

$$\Psi(x) = \min_{i=1,\dots,N} \{t_i + \delta(x, x_i)\} \quad (6.1)$$

where  $\delta(x, x_i)$  is the travel time from  $x$  to  $x_i$  defined as

$$\delta(x, x_i) = \min_{\gamma} \left\{ \int_0^1 \frac{1}{\rho(\gamma(t))} \left\| -\mathbf{G}^{-\frac{1}{2}}(\gamma(t))\gamma'(t) \right\| dt; \right. \\ \left. \gamma \in C^1([0,1], \bar{\Omega}), \gamma(0) = x, \gamma(1) = x_i \right\} \quad (6.2)$$

where  $\mathbf{G}$  is the tensor of effective conductivities and  $\gamma(t)$  is a curve describing the fastest path from point  $x$  to  $x_i$ . Once we assume that the points  $x$  and  $x_i$  are located within a local region of myocardium which is described by a constant values of  $\mathbf{G}$  and  $\rho$ , then the fastest path in Euclidean space is the length of a straight line (or the shortest path) between these two points and the travel time is then given by

$$\delta(x, x_i) = \left\| (\rho\sqrt{\mathbf{G}})^{-1}(x_i - x) \right\| = \|\mathbf{G}'_v(x_i - x)\| \quad (6.3)$$

Since  $\delta(x, x_i)$  represents the travel time and  $(x_i - x)$  represents the distance, then  $\rho\sqrt{\mathbf{G}}$  stands for the local velocity tensor (which is for one-dimensional case in agreement with (3.5)).

## 6.1 The finite-element discretization

A linear finite-element approximation was used to solve the eikonal equation. The structured grid was uniformly tetrahedralized and the activation time was given as the finite-element function in every tetrahedron. The simplified local equations were then solved by the Hopf-Lax formula [26] and the Golden section search method [27]. The resulting system of nonlinear equations was solved by two iterative methods that we adapted to our needs, namely the "Jacobi iterative method" (JIM) and the "Fast iterative method" (FIM) [28]. The idea of the iterative methods is to compute the activation time at each iteration step and to compare the newly computed value against the value from the previous iteration step. If the absolute value of the difference between the new and old value is below some tolerance, then the solution has converged and the algorithm stops to execute.

Around each node in the computational domain ( $n_c \in \Omega_h$ ), an agglomerate  $\omega_c$  was created (see Figure 6.1). As the agglomerate is called a collection of  $m \in \langle 1,8 \rangle$  tetrahedra sharing the node  $n_c$  as their central node. The agglomerates play important role in the proposed eikonal solver, since the solution (activation time) was always evaluated per agglomerate basis. In order to compute the activation time at  $n_c$  of each agglomerate a collection of minimization problems was solved. The idea of the minimization was to localize virtual node on the agglomerate surface, the travel time from which to  $n_c$  was minimal. This virtual node and the travel time from it to  $n_c$  were evaluated separately for each of the agglomerate's tetrahedra. Within each tetrahedron, the solution was approximated using the known activation times at the other three nodes of the tetrahedron and assuming  $\mathbf{G}$  and  $\rho$  be constant within the tetrahedron.

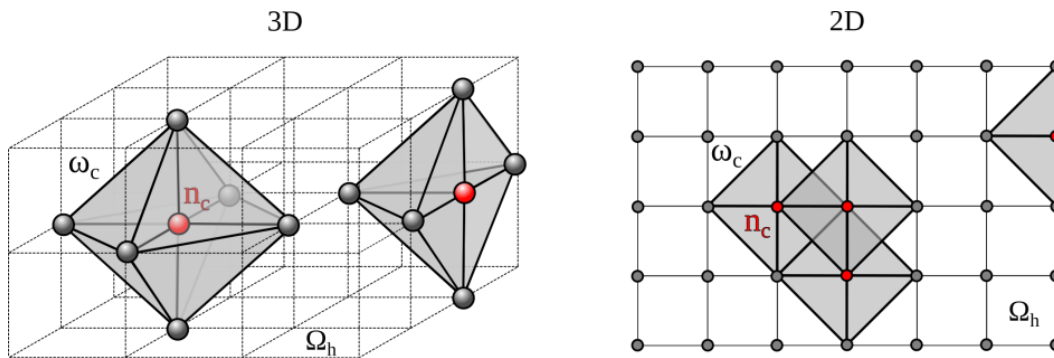


Figure 6.1: On the left: 3D representation of two different agglomerates  $\omega_h(n_c)$  formed by tetrahedra sharing the node  $n_c \in \Omega_h$ . On the right: 2D representation of four agglomerates.

During the kernel execution individual threads operated on individual tetrahedra, and the groups of eight consecutive threads operated on agglomerates. In more detail, the first eight threads computed the solution at the central node of agglomerate with index zero, the next eight threads computed the solution at central node of agglomerate with index one, and so on. After the solution within the tetrahedron was obtained, each thread within the agglomerate sent its solution to the shared memory through the atomic function. This atomic function served as a filter that saved into the shared memory the minimum activation time among all in the agglomerate. Once the minimal solution was obtained the content of the shared memory was copied into a global memory array that at the end of the kernel execution held newly computed solutions. Consequently, after the synchronization with the CPU, the convergence of the solution was checked. Once the solution converged the iteration process was stopped.

## 6.2 The data structures

Based on the above mentioned agglomerate-based assumptions of the thread organization, the data structures supporting the coalesced memory accesses of running threads were created. It is out of the scope of this Summary to discuss all tailored data structures proposed for efficient use on the GPU. Nevertheless, the main idea is captured in Figure 6.2, where chosen data structure used to hold the indices of the nodes of all tetrahedra in the computational domain is depicted. Notice that the elements in the data structure are stored and also fetched per agglomerate basis. Hence, the data structure supports coalesced memory accesses of running threads during the kernel execution. In Figure 6.2 the  $N$  represents number of nodes in the computational domain.

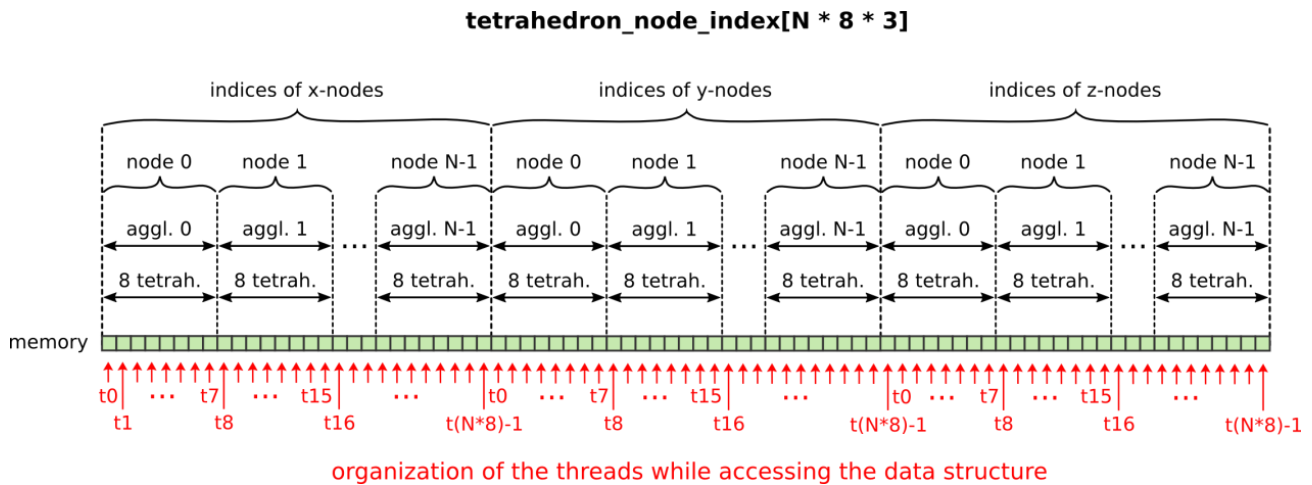


Figure 6.2: Schematic view of the data structure used to keep the indices of the tetrahedron nodes. In red is depicted the organization of the GPU threads while accessing the data structure.

## 6.3 Jacobi iterative method

The JIM solved the eikonal equation at all nodes of the computational domain at each iteration, thus the activation times were computed even at the nodes that were far away from the excitation front. In the preprocessing step, the boundary conditions (the early activation sites) were set on corresponding mesh

nodes, and the values of the rest of the mesh nodes were set to infinity. In the iteration step the activation times were iteratively computed until the solution converged.

#### 6.4 Fast iterative method

In contrast to the JIM, the FIM solved the eikonal equation selectively on the mesh nodes. The solution was iteratively computed only at the nodes laying on the surface of propagating excitation wavefront.

In the preprocessing step, the boundary conditions (the early activation sites) were set on the grid, and the values of the rest of the grid nodes were set to infinity. Next, the six neighbors (in the cardinal directions) of the early activation site nodes were added to the list of active nodes (LAN). In the iteration step only the activation times at the nodes in LAN were updated. The LAN was reevaluated at each iteration step. The nodes were added to or removed from the LAN based on a convergence measure. The iteration procedure was repeated until the LAN was empty.

### 7 Numerical implementation of the ECG computation

The eikonal model provides a field of ventricular activation times  $\Psi(x)$ . To compute the surface ECGs, a lead field was used, one such lead field for each of the twelve standard ECG electrodes. The computation of each ECG lead potential  $V(t)$  at time  $t$  was based on the lead field theory [8], [9] and the bidomain representation of the cardiac sources

$$V(t) = \int_{\Omega} \nabla V_m(x, t) \cdot \mathbf{G}_i(x) \nabla Z(x) dv \quad (7.1)$$

where  $\Omega$  is the heart domain,  $dv$  is elementary volume of the heart domain,  $x$  is the position in the heart,  $V_m(x, t)$  is the transmembrane potential at position  $x$  and time  $t$ ,  $\mathbf{G}_i(x)$  is the intracellular conductivity tensor and  $Z(x)$  is the lead field of the specific ECG lead. The lead field was created by a unit current applied in the two electrode locations

$$\nabla \cdot (\mathbf{G} \nabla Z) = \begin{cases} -1 & \text{at the positive electrode,} \\ 1 & \text{at the negative electrode,} \\ 0 & \text{elsewhere.} \end{cases} \quad (7.2)$$

where  $\mathbf{G} = \mathbf{G}_i + \mathbf{G}_e$  is the bulk conductivity tensor of the body ( $\mathbf{G}_i$  vanishes outside the heart) [29]. (In this procedure a potential field is established in the torso and the gradient of this potential field at any point in the heart region is termed as the lead field  $\mathbf{Z}$  ( $\Omega\text{m}^{-1}$ ) of a given electrocardiographic lead [9].) Equation (7.2) was solved for  $Z$  with R-D model [3], [4], using the patient-specific heart and torso models created as described in [30]. Both the lead field and the dipole sources were computed with fully anisotropic conductivity values. To obtain  $V_m(x, t)$  from  $\Psi(x)$  a predefined action potential waveform  $U(t)$  was used

$$V_m(x, t) = U(t - \Psi(x)) \quad (7.3)$$

Two methods for the computation of the ECGs were implemented, namely the "Simple method" (SM) and "Fast method" (FM). These methods will be discussed in the upcoming chapters.

## 7.1 The data structures

Since the transmembrane potentials as well as the lead field values are defined at cubes nodes, and the conductivities are defined at cubes, it is convenient to let the threads to evaluate the ECGs per cubes, not per nodes as it was in case of the eikonal solver. Hence, we let the consecutive threads to operate on consecutive cubes of the mesh. Based on this assumption the cube-based data structures were designed for the computation of ECGs. Again, it is out of the scope of this Summary to discuss all tailored data structures proposed for efficient use on the GPU. Nevertheless, in Figure 7.1 chosen data structure used to hold the indices of eight nodes of all cubes in the computational domain is depicted. Again this data structure supports coalesced memory accesses of running threads during kernel execution.

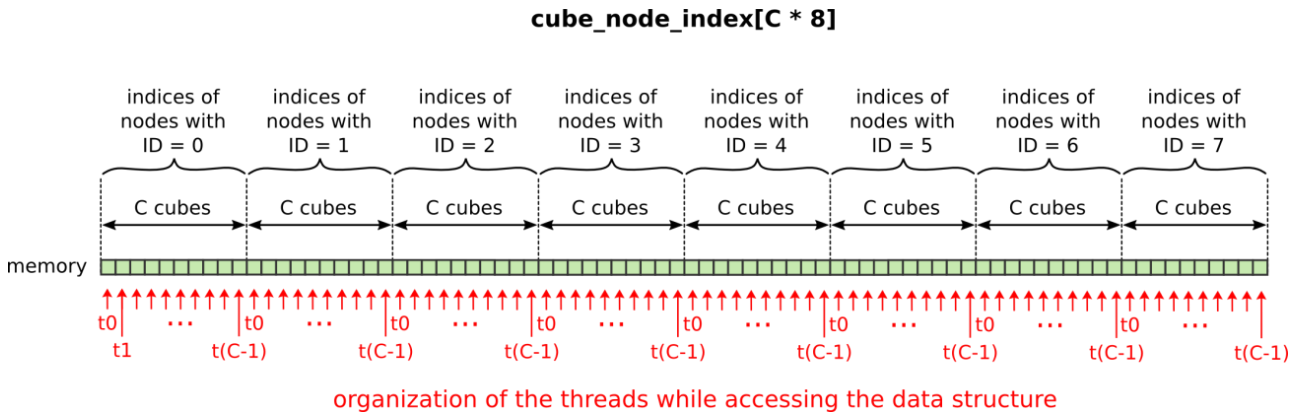


Figure 7.1: Schematic view of the data structure used to keep the indices of the cube nodes ( $C$  is number of all cubes). In red is depicted the organization of the GPU threads while accessing the data structure.

## 7.2 Simple method

In the SM directly the integral in (7.1) was evaluated. Each cube was assigned to an individual thread, and each thread was updating the local contribution of one cube to the ECG. In order to compute an ECG sample for fixed time instant  $t$ , hence the  $V(t)$ , the contributions from all the cubes for that instant were summed up. Our implementation performed an atomic summation directly in the global memory. Further, since standard 12 ECG leads were computed, and the computation of individual leads is independent from each other, also parallel CUDA streams were integrated into the code. Each stream computed one ECG lead. The aim was to support a grid level concurrency by running multiple kernels in parallel, and thus to keep the GPU busy as much as possible. Moreover, in order to support also overlapping of the data transfers with the kernel execution, all transfers between the CPU and GPU were realized using asynchronous functions.

### 7.3 Fast method

Thanks to the coarea formula [31] the equation (7.1) can be rewritten as the convolution of two functions as follows

$$V(t) = (U' * w)(t), \quad w(t) = \int_{S_t} \mathbf{n}(x) \cdot \mathbf{G}_i(x) \nabla Z(x) dS_t \quad (7.4)$$

where  $U'(t)$  indicates the temporal derivative of the action potential waveform and  $S_t$  is the surface of the excitation wavefront at time  $t$  with  $\mathbf{n}(x)$  being its normal.

The computation of the ECG proceeded in two steps. First, the  $w(t)$  function was evaluated with the marching cubes (MC) algorithm [32] that was modified to run on the GPU. Each cube was assigned to an individual thread, and each thread was updating the local contribution of one cube to the  $w(t)$  function. However, this contribution was computed only for those time steps for which the excitation wavefront intersected the cube. The MC algorithm based on the known activation times resident at the eight cube nodes returned the triangulation of the excitation front in particular cube (see Figure 7.2). Second, after the synchronization on the CPU, the convolution itself was computed by another kernel on the GPU. Similarly to the Simple method, the CUDA streams were also included into the computation of ECGs. Each CUDA stream evaluated one ECG lead.

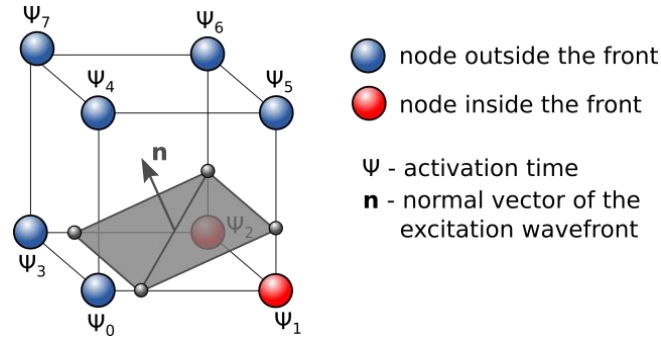


Figure 7.2: Marching cubes – localization of the excitation wavefront in between nodes of opposite classification.

## 8 Results and discussion

In this section first the computational power of the GPUs on a relatively small computational problem compared to the simulations of the electrical activity of the whole heart is examined. In particular, the speedup of a parallel real-time multichannel ECG filtration running on the GPU is evaluated. Next the attention is focused on the proposed forward model. The performance of the proposed eikonal solver and ECG solver in terms of their runtimes on the GPU is discussed. Afterwards the activation times and ECGs computed by the parallel solvers are compared with their counterparts obtained from an R-D model that served as a reference. Finally, a possible practical application of the eikonal solver is shown. The eikonal solver combined with an inverse optimization procedure is used to estimate the position of early activation site and the regional conduction velocities in the heart. The optimization procedure makes use of the difference between simulated and measured activation times.

## 8.1 Real-time multichannel ECG signal processing on GPU

Before the parallel GPU kernels were integrated into the proposed forward model consisting of tens of thousands of elements, the suitability and computational efficiency of the GPU was tested on a smaller ECG processing task where only thousands of the GPU threads did the computations.

Three programming modules that are commonly incorporated into the real-time ECG signal processing procedure were created, namely the data formatting module, data saving module and filtration module. Since the filtration module was computationally the most intensive it was parallelized and designed for the execution on the GPU. The filtration module eliminated the ECG baseline wandering using a high-pass finite impulse response filter with the impulse response length of 4065 samples. The filter was realized in the frequency domain using the convolution theorem of the discrete Fourier transform. To ensure continual ECG filtration a well-known overlap-save block filtering algorithm [33] was used. The implementation details are documented by Kal'avský and Tyšler in [34].

In the experiments the runtimes of all three modules were measured on the CPU, and the runtime of the filtration module was evaluated also on the GPU. The performance of proposed modules was tested on one CPU core of the Intel core i7-875K (4 cores, 2.93 GHz, 4 GB DDR3) and the performance of the parallelized module on NVIDIA GeForce GTX 480 GPU (480 cores, 1.4 GHz, 1536 MB GDDR5). During the experiments 67 simulated ECG signals from a signal generator were sensed by the high-resolution multichannel ECG mapping system ProCardio-8 [35] using the sampling frequency of 2000 Hz and 22-bit sample resolution. The signal matrix entering periodically the filtration was of the size 67 x 4096 samples. The threads in the parallel version of the data filtration module computed 67 forward FFTs and consequently 67 inverse FFTs in parallel using the CUFFT GPU-based library [36]. Moreover, for the elementwise multiplication of DFTs of input sequence and the impulse response, the kernel with 67 x 4096 running threads was created, and each thread of this kernel computed one element of the output matrix. The runtimes of individual program modules are depicted in Figure 8.1.

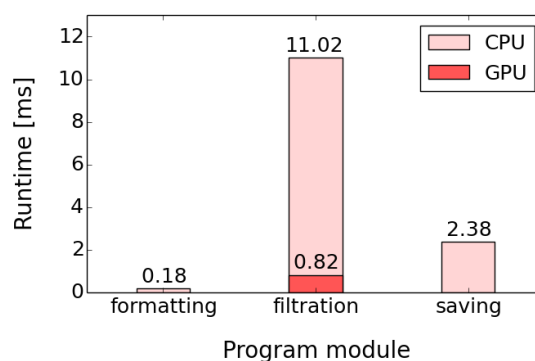


Figure 8.1: Runtimes of individual program modules.

As it can be seen in Figure 8.1, thanks to the thousand of threads executing in parallel the total runtime needed for the multichannel filtration decreased from 11.02 ms to only 0.82 ms what represents 13.4 fold speedup and accounts for 93% saving of the serial runtime of the filtration module. For the sake of completeness it is important to mention that the implemented high-order digital filter has more or less

illustrative character because the time delay of this filter is approximately 1 second, thus its real-time nature can be debatable. However, this simple experiment demonstrated computational power of the GPU. Thanks to the massively parallel algorithms running on the GPU the computation time of the filtration decreased approximately by one order.

## 8.2 Forward modeling results

In this chapter the term "Propeiko" will serve as the synonym of the proposed forward model consisting of the eikonal solver and ECG solver. First the runtimes of both Propeiko solvers are discussed, and consequently the activation times and ECGs computed by Propeiko are compared with their counterparts obtained from a large-scale R-D model called Propag [3], [4], that was used as reference. At this point it is important to point out two facts. First, Propag similarly to Propeiko enabled to solve the desired output on a structured grid of the ventricular model. Second, similar patient-specific ventricular and torso geometries were used in order to compare corresponding outputs of both models. Small differences between geometries were caused by downsampling of the 0.2 mm ventricular mesh used by Propag to the 1.0 mm ventricular mesh used by Propeiko. In practice, monodomain equation of Propag was used for the computation of action potentials (and hence also activation times) on the 0.2 mm mesh and the obtained activation sequence was downsampled to a 1.0 mm mesh for the comparison with Propeiko. The computation of the ECGs by both models was performed on a torso model with 1 mm resolution. In Propag the bidomain equation was used for the computation of ECGs and the gradients of action potentials computed by monodomain equation were used as the currents. For the computation of the lead fields, the bidomain equation was used, with the currents applied in the corresponding electrode positions on the torso surface.

The ventricular geometries used in the experiments consisted of the layered structure of substances mentioned in the Chapter 5.1 and shown in Figure 5.2. Each ventricular model consisted of eight layers. Four transmural layers called *fast*, *endo*, *mid*, and *epi* were created in the right ventricle (RV) and similar four transmural layers were created also in the left ventricle (LV). During the experiments the conduction velocity in the *fast* layers of both ventricles was set higher than in the remaining layers. For patient 3 the conduction velocity was set higher only in the *fast* layer of the RV. The values of parameters used in the simulations are listed in Appendix A of proposed thesis. In Table 8.1 is provided relevant information about the used ventricular meshes.

Patient	Mesh dimension	Number of nodes	Number of tetrahedra	Number of cubes
1	127 x 124 x 187	289 252	2 314 016	230 968
2	148 x 118 x 179	350 584	2 804 672	290 166
3	130 x 116 x 161	248 140	1 985 120	202 942
4	109 x 92 x 157	222 951	1 783 608	187 534

Table 8.1: Specification of the ventricular meshes used in the experiments (mesh dimension correspond to the dimension of the whole heart including atria).

Both proposed solvers were implemented in the C++ and CUDA C/C++ languages and are destined to execute on the CUDA GPUs. The only required external library was Thrust [37], included in CUDA toolkit. In all experiments single precision floating point representation of numbers was used.

Both solvers were tested on two different Nvidia GPUs. One of them was a low-end (LE) GPU GeForce GT 650M on a personal laptop, and the another one was a high-end (HE) GPU Tesla K20X on a node of the supercomputer Piz Daint at CSCS [38]. Parameters of both GPUs are given in Table 8.2. Finally, in Table 8.3 are listed parameters of another supercomputer at CSCS called Piz Dora [38] that was used to run the R-D model.

GPU	Number of cores	Core clock	Main memory bandwidth	Main memory size	Peak performance (single precision)
LE	384	0.950 GHz	80 GB/s	2 GB	0.73 Tflops
HE	2688	0.732 GHz	250 GB/s	6 GB	3.95 Tflops

Table 8.2: Specification of the GPUs used in experiments.

Model	Number of compute nodes	Number of cores per node	Core clock	Memory bandwidth per node	Memory size per node	Peak perform.
Cray XC40	1256	36	2.1 GHz	137 GB/s	64 GB	1.509 Pflops

Table 8.3: Specification of the supercomputer Piz Dora at CSCS.

### 8.2.1 Comparison of eikonal solver runtimes

In Figure 8.2 are shown the runtimes (in seconds) of Jacobi iterative method (JIM) and Fast iterative method (FIM) on the LE and HE GPU. Important observation is that both methods enabled to compute the activation sequence in the ventricles in the order of seconds. Moreover, the runtimes of the FIM executed on the HE GPU were below one second.

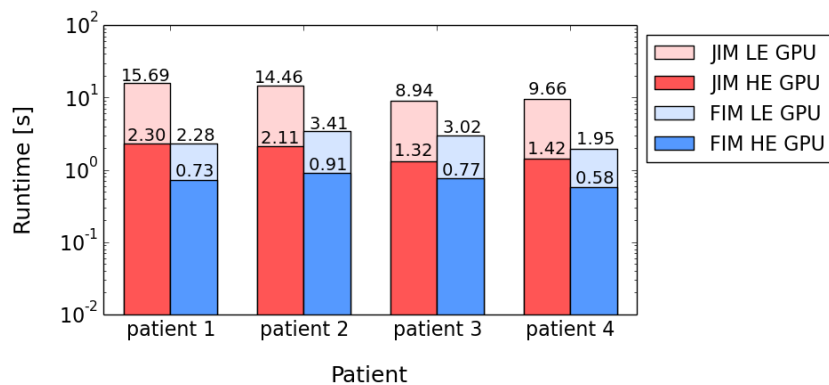


Figure 8.2: Runtimes (in seconds) for JIM and FIM on the LE and HE GPU. (Logarithmic scale is used on the vertical axis.)

A positive feature of the JIM is its scaling. The JIM ran on the HE GPU almost 7-times faster than on the LE GPU, which represents almost ideal scaling since the HE GPU has exactly 7-times more cores than the LE GPU. On the other side, the disadvantage of this method is that at each iteration it evaluates the activation times at all nodes of the ventricular mesh, thus also at the nodes that are far away from the excitation front. In order to avoid this problem the FIM was implemented. The FIM allowed evaluating of the activation times only in a narrow band of nodes on the excitation front. As it is shown in Figure 8.2, the runtimes of the FIM (for all four patients) were below 3.5 seconds on the LE GPU and below 1 second on the HE GPU. Compared to the JIM, 3 to 7-fold speedup was achieved on the LE GPU and 2 to 3-fold speedup was achieved on the HE GPU. This means that the FIM enables to obtain the activation sequence also on a common laptop within a few seconds, and moreover, execution times applicable for real-time simulations may be reached on the HE GPU. The bottleneck of the FIM is its scaling. The FIM ran on the HE GPU on average only 3.5 times faster than on the LE GPU. Such a behavior may be explained by the fact, that a relatively small number of threads did computations at each iteration.

It is very interesting to compare the runtimes of the proposed eikonal solver with the runtime resulting from the simulation of ventricular action potentials by Propag (reference R-D model). For sure, the Propag runtimes depend on the number of CPU cores used and their speed. The average runtimes achieved when running Propag on Piz Dora (see Table 8.3) with number of processes around 800 (1 thread per process) are discussed in the following section. The monodomain simulations of ventricular depolarization on a mesh with resolution of 0.2 mm took around 10 minutes. The corresponding bidomain simulations would run about 20 times longer [3], thus around 200 minutes. In addition tens of gigabytes of memory are required to run these simulations. From this discussion it is important to realize the significant performance difference between the proposed eikonal solver and the more realistic R-D model. It is important to realize that the eikonal solver enables to simulate activation sequence in the heart ventricles even on a personal laptop equipped with 2 GB of GPU DRAM in about 3 seconds.

Additional discussion about the impact of the warp scheduling, atomic operations, texture memory and tailored data structures on the performance of the proposed eikonal solver, as well as the comparison of proposed eikonal solver with recently developed eikonal solver of Fu et al. [39] (destined for solving the eikonal equation on three-dimensional, unstructured, tetrahedral domains), can be found in proposed thesis.

### 8.2.2 Comparison of ECG solver runtimes

The runtimes (in seconds) of the Simple method (SM) and Fast method (FM) on the LE and HE GPU are shown in Figure 8.3. Both methods computed 600 ms long signals of the 12-lead ECG. Figure 8.3 shows the runtimes of both methods assuming the ECG resolution of 0.5 ms and 1.0 ms. Important observation is that the SM method runtime on the GPU was of the order of seconds, while the FM runtime was of the order of tens of milliseconds.

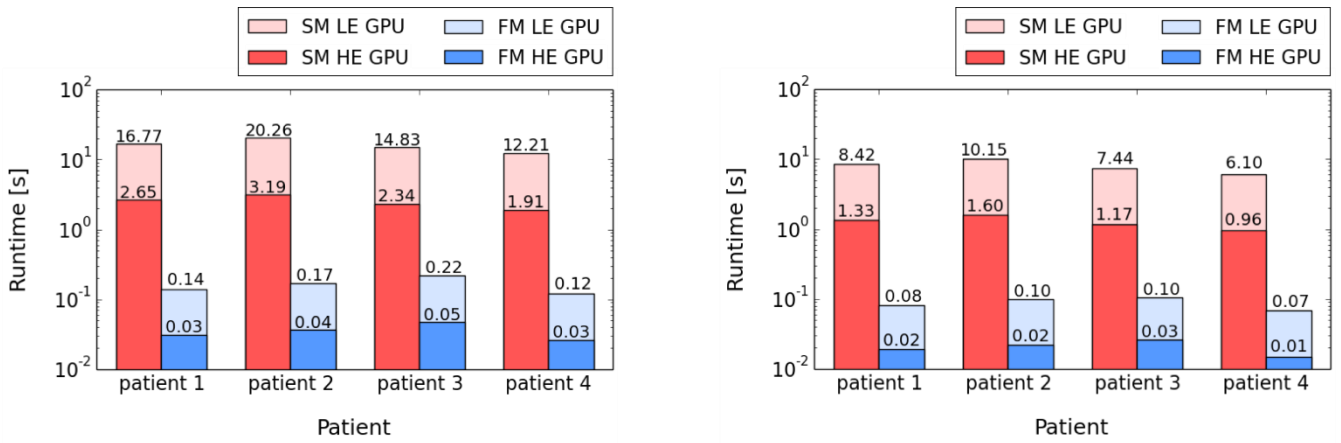


Figure 8.3: Runtimes (in seconds) of SM and FM on the LE and HE GPU. Results for ECG resolution of 0.5 ms and 1.0 ms are shown on the left and right, respectively. (Logarithmic scale is used on the vertical axis.)

The runtime of the SM on the HE GPU (for all four patients) was below 3.2 seconds for 0.5 ms ECG resolution and below 1.7 seconds for 1.0 ms ECG resolution. The SM scaled very well on the HE GPU with an average scaling factor around 6.35.

Now, let us have a look on the runtimes of the FM. As it can be seen in Figure 8.3, the computation of the 12-lead ECG took only tens of milliseconds on both GPUs. The runtimes of the FM, for all four patients and for the ECG with the higher of the two tested resolutions, were below 220 milliseconds on the LE GPU and below 50 milliseconds on the HE GPU. The runtimes of the FM for the ECG with the lower of the two tested resolutions were below 110 ms on the LE GPU and below 30 milliseconds on the HE GPU. Purely from the computational point of view, the FM is in average more than 80 times faster than the SM. The scaling of the FM was not optimal. The FM ran on the HE GPU on average only 4.5 times faster than on the LE GPU. Not optimal scaling was likely caused by the fact that different warps required different number of clock cycles to finish their execution. As a consequence of unbalanced execution times of different warps in the computational domain, the linear scaling of the FM was broken.

It is further worthwhile to mention that both proposed ECG solvers take as one of their inputs the lead field. On the one hand, from the computational point of view of the ECG solver, the precomputed lead field represents a beneficial input parameter. On the other hand, the computation of the lead field itself might be considered as the bottleneck of proposed ECG solvers. Each time the conduction velocities of the ventricular or torso regions are changed, the lead field has to be recomputed by the bidomain model. The computation of the lead fields for the standard 12 ECG leads takes on Piz Dora (with around 800 processes and 1 thread per process) approximately 3 minutes. However, once the lead field is available, the proposed ECG solvers can be effectively used to simulate the ECGs. If it is necessary to adjust the conduction velocities only in the ventricles, it is to a certain extent possible to avoid the recomputation of the whole lead field. The desired value of the conduction velocity in the ventricles can be set easily by tuning the membrane parameter  $\rho$  (see (3.5)).

Similarly like in the previous chapter it is interesting to compare the runtimes of the proposed ECG solver with the runtime resulting from the simulation of ECGs by Propag. As it was already mentioned, action potentials generated by the monodomain equation were used for the computation of the ECGs in Propag. The

simulation of the action potential of 500 ms length (the depolarization plus the repolarization) took around 22 minutes. Once the monodomain simulation was done, the bidomain simulation was performed to compute the potential field everywhere in the torso. The computation of this potential field took around 14 minutes and required around 350 GB of memory. The last step, the computation of 12-lead voltages from known potentials at specific nodes on the torso surface took obviously negligible time. Again, the runtimes on Piz Dora (see Table 8.3) with around 800 processes were discussed. To summarize, for Propag it took minutes to simulate the standard 12-lead ECG, while for Propeiko it took only a few seconds.

Additional discussions about the impact of the warp scheduling, atomic operations, texture memory and tailored data structures on the performance of the proposed ECG solver can be found in proposed thesis.

### 8.2.3 Comparison of activation times computed by Propag and Propeiko

As it was already mentioned in Chapter 8.2, the activation times were compared on four patient-specific geometries with 1 mm resolution and with model parameters given in Appendix A of proposed thesis. The activation times were compared in terms of the absolute error at corresponding ventricular nodes. The results for Patient 1 are shown in Figure 8.4. This figure shows a three-dimensional view of the activation sequence and the distribution of the absolute error. The plotted results for remaining three patients can be found in proposed thesis. The most relevant results for all 4 patients are summarized in a compact form in Table 8.4.

Patient	Absolute error [ms]		Number of nodes [%]	
	minimum	maximum	Absolute error $\leq 5$ ms	Absolute error $\leq 10$ ms
1	$2.67 \times 10^{-5}$	17.31	77	96
2	$3.05 \times 10^{-5}$	30.08	69	92
3	0.0	23.39	63	90
4	$4.58 \times 10^{-5}$	14.56	84	99

Table 8.4: Absolute error (in milliseconds) between Propag and Propeiko activation times.

The results showed that the absolute errors of the activation times varied between 0.0 and 30.08 ms. The absolute error of the order of tens of milliseconds is quite high, when assuming normal duration of the depolarization (QRS complex in ECG) about 80 ms. However, closer evaluation of the absolute error at individual ventricular nodes showed that, the absolute error was equal or less than 5 ms in average at 73% of nodes, and equal or less than 10 ms at 94% of nodes. Visually, the activation sequence computed by Propeiko exhibited similar propagation pattern as the activation sequence computed by Propag. In the three-dimensional distribution of the absolute error no dominant pattern was observed. If we take into account the fact that the computation of the activation sequence using Propeiko takes a few seconds on a personal laptop in contrast to minutes required to obtain corresponding solution on HPC machines using Propag, we may consider this approximation of the activation sequence as acceptable.

To reason the differences between the Propag and Propeiko activation times thoroughly, additional experiments are required. In any case, besides the numerical errors of both methods, other possible reasons influencing the results could be the small differences in the fiber orientation and the inherent structure

between the full and the downsampled ventricular geometries. In Propeiko the material properties and the fiber orientation are defined directly on the 1.0 mm mesh. On the other hand, in Propag the material properties and the fiber orientation are defined on the 0.2 mm mesh, and this finer mesh is used also for the simulation of the action potentials. The extracted activation times are then downsampled and saved on the 1 mm mesh. Indeed, these slight dissimilarities could affect the solution.

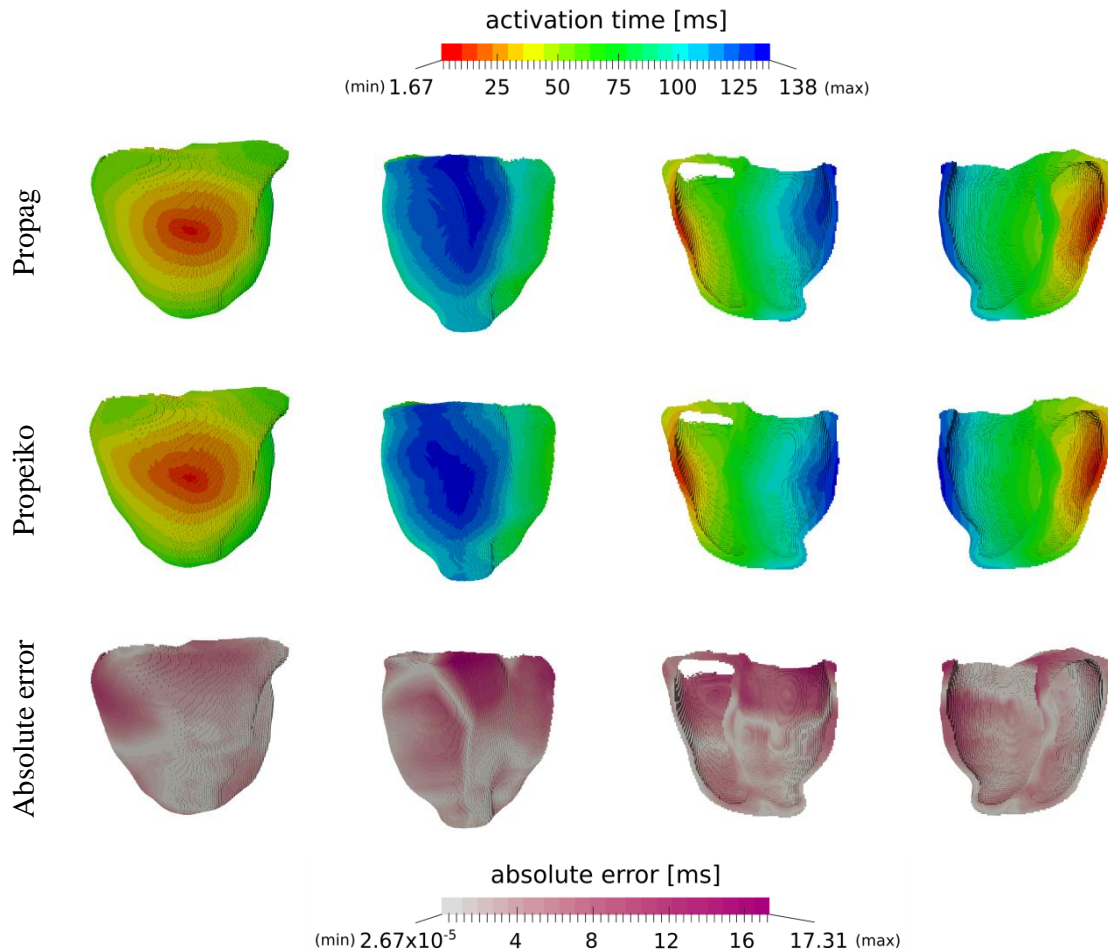


Figure 8.4: Comparison of the activation times computed by Propag and Propeiko for Patient 1. In the upper part of the figure the earliest epicardial activation of the right ventricle, the latest epicardial activation of the left ventricle, and the endocardial activation of both ventricles is shown from left to right. (Two complementary longitudinal sections across the heart ventricles and septum are used to show the endocardial activation.)

#### 8.2.4 Comparison of ECGs computed by Propag and Propeiko

The ECGs were computed according to the standard 12-lead ECG definitions (see [9]), hence three bipolar limb leads ( $I$ ,  $II$ ,  $III$ ), three augmented unipolar limb leads ( $aVR$ ,  $aVL$ ,  $aVF$ ), and six unipolar precordial leads ( $V_1$  to  $V_6$ ) were computed. Propag used bidomain equation to compute the ECGs, while Propeiko used the lead field approach. In order to compare Propag and Propeiko ECGs four assessment criteria were evaluated: an absolute error (ABS), RMS error (RMS), RMS relative difference (RMS\_RD), and correlation coefficient (CC). These four criteria were computed separately for the depolarization and repolarization

segment of each of the 12 leads. For the ECGs computed using the Simple method, both, the depolarization (DEPO SM) and repolarization (REPO SM) segment were evaluated, while for ECGs computed using the Fast method only the depolarization segment (DEPO FM) was evaluated. The length of the DEPO segment was derived from the minimum and maximum activation time. The REPO segment started right after the DEPO segment and was terminated by the last simulated ECG sample (the sample corresponding to 500 ms).

In this Summary only the observed values of the RMS\_RD and CC for DEPO SM, DEPO FM, and REPO SM segments are plotted in Figure 8.5 to Figure 8.7, respectively. However, these plotted results are supplemented by Table 8.5, in which the minimum (min), maximum (max) and average (avg) values of all four evaluated criteria across all patients and all leads are summarized. The simulated ECGs for Patient 1 are shown in Figure 8.8, hence one can also visually check the polarity, timing, and shape of computed ECGs. The simulated ECGs for remaining three patients can be found in proposed thesis.

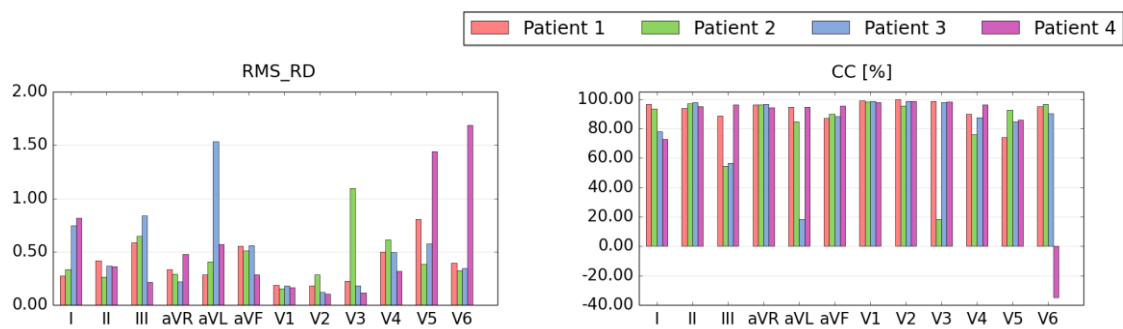


Figure 8.5: DEPO SM segment of standard 12-lead ECG – Comparison of ECGs computed by Propeiko and Propag.

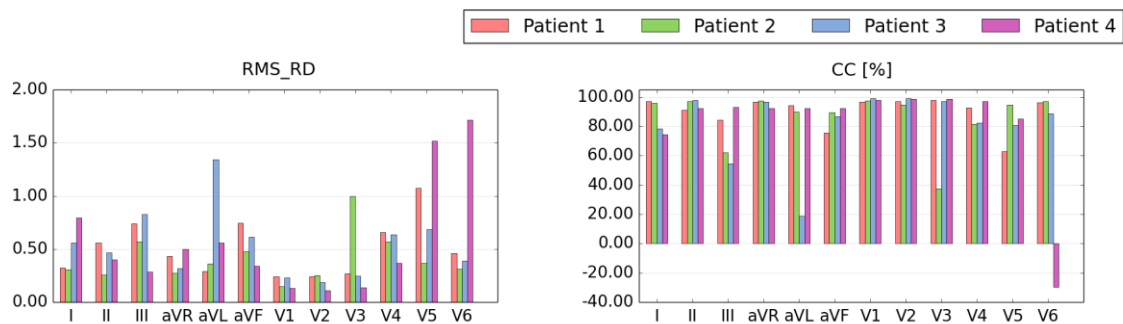


Figure 8.6: DEPO FM segment of standard 12-lead ECG – Comparison of ECGs computed by Propeiko and Propag.

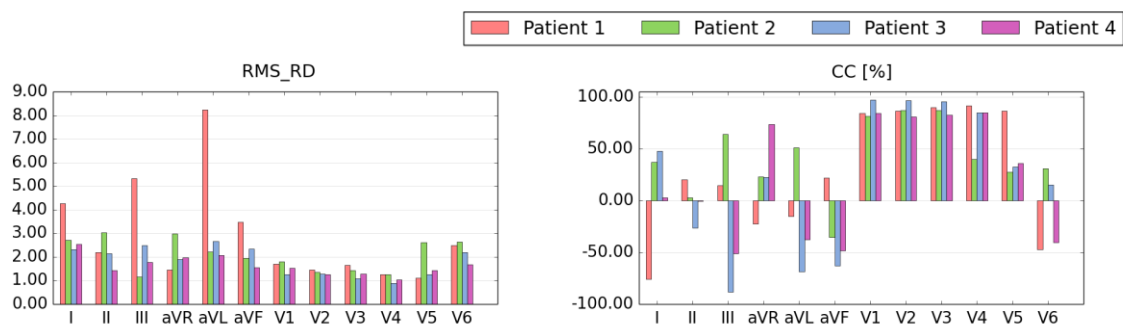


Figure 8.7: REPO SM segment of standard 12-lead ECG – Comparison of ECGs computed by Propeiko and Propag.

Segment	ABS [mV]			RMS [mV]			RMS_RD			CC [%]		
	min	max	avg	min	max	avg	min	max	avg	min	max	avg
DEPO SM	0.14	0.69	0.37	0.06	0.29	0.15	0.10	1.69	0.47	- 34.97	99.69	85.23
DEPO FM	0.15	1.03	0.39	0.05	0.39	0.17	0.11	1.71	0.51	- 29.48	99.16	85.05
REPO SM	0.12	2.65	0.63	0.05	0.91	0.24	0.89	8.23	2.11	- 88.08	96.87	27.98

Table 8.5: Standard 12-lead ECG – Comparison of ECGs computed by Propeiko and Propag (all four patients, all 12-leads).

The QRS complex (DEPO segment) computed using both, Propeiko SM and FM exhibited good compliance with the QRS complex generated by Propag. For the DEPO FM segment following average values of evaluated criteria were found: ABS of 0.39 mV, RMS of 0.17 mV, RMS\_RD of 0.51, and CC of 85.05 %. The DEPO SM segment exhibited slightly better results than the DEPO FM segment. In general, in majority of QRS complexes the shape and polarity matched what was best quantified by the CC. However, as it can be seen in Figure 8.5 and Figure 8.6, also one clear outlier in lead V6 of Patient was found, and two leads with CC below 40%, namely aVL in Patient 3 and V3 in Patient 2 were found. Visual inspection of these leads showed that the polarity of lead V6 was reversed, and that in the aVL and V3 lead, the Q wave was of the opposite polarity.

The experiments further showed variations in the QRS complex amplitude. We found the RMS\_RD and ABS to be the most sensitive indicators of amplitude differences. The ABS varied from 0.14 to 1.03 mV and RMS\_RD from 0.10 to 1.71. From the quantitative point of view, the RMS\_RD and ABS acted as two complementary indicators. The RMS\_RD more clearly signaled the differences in lower amplitude leads, thus in the majority of simulated leads, while the ABS better indicated the differences in higher amplitude leads, namely in the precordial leads V1, V2 or V3. Such an observation is reasonable since, the differences between Propag and Propeiko QRS complexes for leads V1, V2 and V3 were relative small when compared with the amplitudes of these leads, and hence the RMS\_RD smoothed these differences. To conclude, in the majority of leads, the DEPO segments generated by Propeiko SM and FM exhibited acceptable differences when compared with Propag depolarization segments.

Let's now have a look on the comparison of the repolarization segments. Following average values of evaluated criteria were found for the REPO SM segment: ABS of 0.63 mV, RMS of 0.24 mV, RMS\_RD of 2.11, and CC of 27.98 %. Clearly, the RMS\_RD and CC signaled bad match between between Propeiko and Propag DEPO segments. Visual inspection of the leads showed differences in the shape, amplitude and polarity of the T wave, what is in agreement with the result plotted in Figure 8.7. In general, the best agreement in terms of the shape was achieved for precordial leads V1, V2 and V3, but on the other side the ABS for these three leads was maximal. In the remaining leads no significant similarities were found. To conclude, the REPO segments generated by Propeiko did not match well with the Propag repolarization segments. Hence, further investigation is required to identify possible error sources. Among the other, numerical errors of both models as well as the small differences in geometry arise as possible candidates.

Nevertheless, the QRS complexes matched quite well. And again, if we take into account the fact that the computation of the QRS complexes using Propeiko takes a hundreds of millisecond on a personal laptop in contrast to minutes required to obtain corresponding QRS complexes by running Propag on a supercomputer,

we may consider these results as very promising and satisfactory. Moreover, we would like to point out that despite many works have been devoted to the numerical simulation of cardiac electrophysiology, only a few of them provided also simulations of the complete 12-lead ECG. To the best of our knowledge, none of the existing approaches combined the eikonal approach and the lead field concept to show realistic 12-lead ECG simulations on patient-specific geometries, as we did.

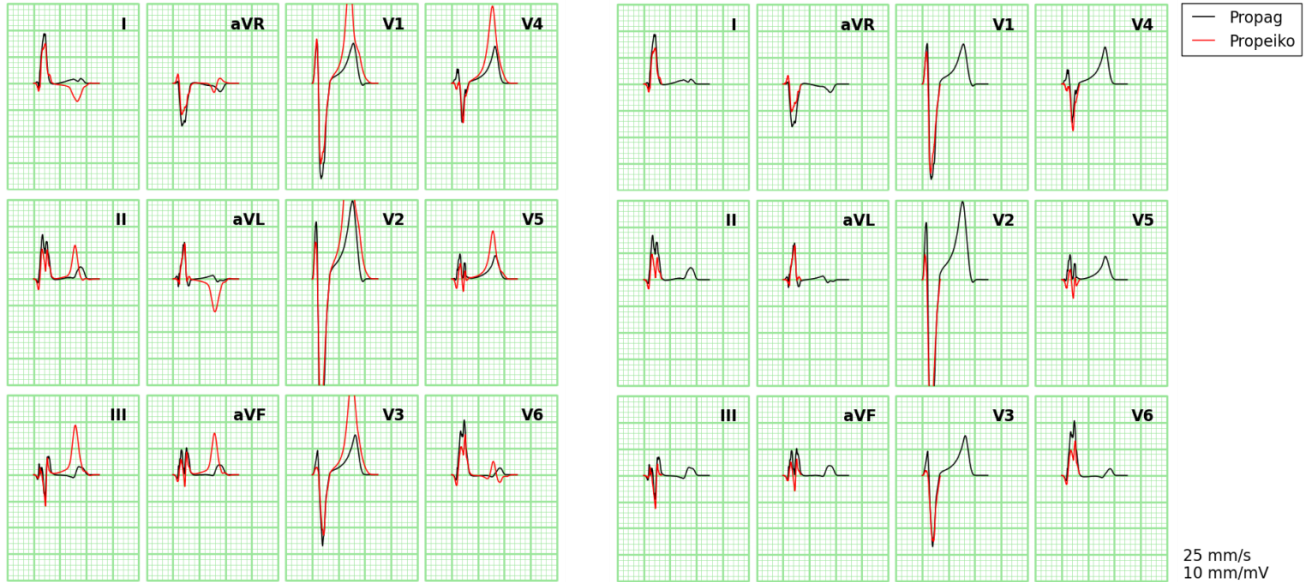


Figure 8.8: Comparison of standard 12-lead ECG computed by Propag and Propeiako for Patient 1. ECGs computed by SM and FM are shown on the left and right side, respectively.

### 8.3 Matching of simulated and measured activation times

In this chapter the initial attempts with the optimization procedure for finding the best agreement between simulated and measured activation times (ATs) are examined. The simulated ATs were generated by the proposed eikonal solver, the measured ATs were obtained by the use of NOGA endocardial mapping system (Johnson & Johnson company). The full set of measured ATs consisted of the ATs measured from the inner surface of the right ventricle (RV), left ventricle (LV), and coronary sinus (CS). For each of the four patients ATs were measured at more than 200 endocardial points.

The experiments were performed by the use of the same ventricular geometries and eight layers of substances as mentioned in Chapter 8.2, hence four transmural layers called *fast*, *endo*, *mid*, and *epi* were assumed in both ventricles. The goal of the optimization procedure was to match the simulated and measured ATs by iterative improving of the locations of single early activation sites (EASs) and by adapting the conduction velocities in two ventricular regions. One of the ventricular regions mimicked the fast Purkinje fibers and was represented by the *fast* RV layer, another one corresponded to the ventricular myocardium and was represented by a composition of the remaining 7 layers. During the optimization procedure the conduction velocities were adjusted by tuning the membrane parameter  $\rho$  only. The conductivity values were kept fixed. The values of the parameters used in the experiments as well as the detail description of complex optimization procedure are described in the proposed thesis. We let the optimization procedure to execute on

a single core of a supercomputer node equipped with Intel Xeon E5-2670 processor (2.60 GHz, 32 GB RAM) and HE GPU with parameters given in Table 8.2. In Figure 8.9 scatter plots showing the relationship between simulated and measured activation times for Patient 1 is depicted. The scatter plots of remaining three patients can be found in proposed thesis.

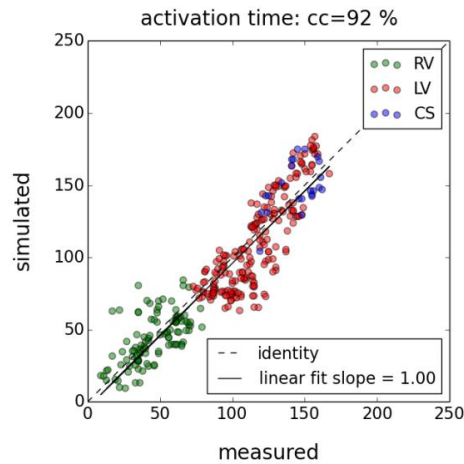


Figure 8.9: Scatter plot of activation times for Patient 1.

The scatter plots of all four patients showed that the activation times were concentrated in the vicinity of the regression line, hence we observed relatively high degree of correlation with CCs from 85 % to 94 %. The slope of the regression line was in all experiments equal to 1.0. For Patient 2 and Patient 3 the regression line was shifted from the identity line more significantly than for Patient 1 and Patient 4. However this shift can be removed by additional tuning of model parameters, namely by setting higher conduction velocities in evaluated regions.

From the computational point of view it is very important that the fine tuning of model parameters for a single patient was achieved in less than 5 minutes. In practice, the eikonal solver was invoked more than one hundred times with different sets of input parameters. If the monodomain simulations were used instead of the eikonal simulation in the optimization procedure, they would run roughly more than half a day.

## 9 Conclusion

A GPU-accelerated fully anisotropic model for the simulation of the activation sequence in cardiac tissue and computation of ECGs was developed. The activation sequence was modeled by the eikonal description of the spread of excitation in the heart. The ECGs were computed by coupling the eikonal approach with the lead field concept and the bidomain representation of cardiac sources. More specifically, to compute the ECGs, first the timing values of the activation sequence were used to obtain the transmembrane potential field from precomputed action potential waveforms, next this transmembrane potential field was scaled by the local tissue conductivities to obtain cardiac sources distributed through the heart, and finally the distributed cardiac sources were related by the precomputed lead fields to the evaluated lead voltages on the body surface.

Simulations performed on four patient-specific geometries with 1 mm resolution showed that the model can simulate the activation sequence and standard 12-lead ECG on a high-end CUDA GPU in a few seconds.

If only QRS complex is of interest, the real-time execution speed may be reached. Simulated activation times and ECGs were compared with their counterparts generated by the R-D model. Satisfactory match was found between activation sequences as well as QRS complexes. The T waves exhibited large dissimilarities, hence deeper study of the parameter setting is required to achieve better agreement. Practical applicability of the model was demonstrated on the inverse procedure that used the measured activation times to estimate the location of a single early activation site and the values of regional conduction velocities. Thanks to the computational speed of the proposed model, the fine tuning of model parameters was completed within a couple of minutes and relatively high degree of correlation between simulated and measures activation times was achieved. The two main limitations of the proposed model are the inability of the eikonal approach to investigate the repolarization phase of cardiac cycle and the need of R-D model to precompute the lead field for individual heart and torso geometry.

To conclude, the main goal of this study was to build a GPU-accelerated fully anisotropic forward model for the simulation of the activation sequence in the cardiac tissue and for the computation of ECGs. In spite of its limitations, the proposed forward model essentially fulfills these requirements and is therefore a good candidate to address the solution of inverse problems.

## 9.1 Contributions of the thesis

Although the fundamental theoretical concepts encompassed in the proposed model are known for many years, this thesis made several contributions to the common knowledge.

First, two methods for solving the three-dimensional anisotropic eikonal equation on structured grid were proposed. These methods extended the versatility of the already existing Jacobi iterative method and Fast iterative method. In order to compute the activation times, three core elements were proposed, each of which is closely tied with a tailored collection of tetrahedra called agglomerate. First, custom tetrahedralization of structured mesh was proposed, next, a unique eikonal solver that takes into account challenging cardiac tissue anisotropy was developed, and furthermore, the data structures necessary for efficient mapping of data to parallel GPU threads were designed. To best of our knowledge, there exist studies dealing with the computational techniques for solving the eikonal equation on structured grids, but they do not discuss a three-dimensional anisotropic eikonal solver and the data structures suitable for the GPUs.

Second, two methods for the computation of ECGs were proposed, namely the Simple method and the Fast method. The Simple method takes into account the transmural heterogeneity in the action potential duration and supports the simulation of both, depolarization and repolarization phase of cardiac cycle (the QRS complex and T wave in ECGs, respectively). The Fast method assumes that the cardiac sources are distributed only on the surface of the excitation wavefront, hence it is suitable for the simulation of the depolarization phase only. Important is that for both methods the fully anisotropic nature of cardiac tissue as well as the anisotropy and heterogeneity of torso regions is incorporated into the computation of the ECGs. From the computational point of view it is worthy to point out the extremely short execution times of the Fast method that even on the low-end GPU generated the 12-lead ECG in tens of milliseconds. Hence, it represents a promising method for speeding up the inverse solutions utilizing the QRS portion of the ECG curve as a feedback parameter. To conclude, although many works have been devoted to the numerical

simulations of cardiac electrophysiology, only a few of them provided also simulations of the complete 12-lead ECG. To the best of our knowledge, none of the existing approaches combined the eikonal approach and the lead field concept to simulate realistic 12-lead ECG, as we did.

Third, we would like to strength that GPU-accelerated forward model was developed. Each of the four above mentioned methods supports massively parallel computations on the GPUs. The scalability tests showed that the proposed algorithms can exploit the performance of the GPUs with higher number of processor cores, what is highly valuable feature with respect to current trends in HPC hardware design. Thanks to the massive parallelism, tailored data structures and thread organization that maintained high computational density, the runtimes in the order of seconds were achieved even on a today's personal laptop equipped with a low-end GPU. When compared with the runtimes of R-D models, a speedup of several orders was achieved. On the other side, the proposed eikonal model solution is just an approximation of the state-of-the-art R-D model solution. Hence, it is important to perceive the proposed model as a computationally fast complementary tool that can be effectively used in various inverse procedures, e.g. to estimate the locations and number of early activation sites and the conduction velocities in the myocardial tissue. The outputs of these inverse procedures can be consequently used as initial guesses in R-D models, by which the final tuning of the heart activation may be performed to identify the diseased regions of the heart. This thesis discussed only an inverse procedure that made use of measured activation time. However the future goal is to estimate the underlying quantities directly from measured ECGs. This is highly relevant because it is not desirable to use cardiac catheters in all patients prior to the choice of treatment. This problem is much broader than the first one, and has to be viewed as a long-term goal.

## Bibliography

- [1] BRAUNWALD, E. Heart Failure. *JACC Heart Fail.* 2013, vol. 1, no. 1, p. 1–20.
- [2] TUNG, L. *A bidomain model for describing ischemic myocardial D-C potentials*. Dissertation thesis. Massachusetts Inst. Technol., 1978.
- [3] POTSE, M. et al. A comparison of monodomain and bidomain reaction-diffusion models for action potential propagation in the human heart. *IEEE Trans. Biomed. Eng.* ISSN 0018-9294, 2006, vol. 53, no. 12 Pt 1, p. 2425–2435.
- [4] KRAUSE, D. et al. Hybrid Parallelization of a Large-Scale Heart Model. *Facing Multicore - Chall. II*. Springer Berlin Heidelberg, 2012. ISBN: 978-3-642-30396-8, p. 120–132.
- [5] POTSE, M. Mathematical Modeling and Simulation of Ventricular Activation Sequences: Implications for Cardiac Resynchronization Therapy. *J Cardiovasc. Transl. Res.* ISSN 1937-5387, 2012, vol. 5, no. 2, p. 146–158.
- [6] FRANZONE, P. C. - GUERRI, L. - TENTONI, S. Mathematical modeling of the excitation process in myocardial tissue: influence of fiber rotation on wavefront propagation and potential field. *Math. Biosci.* ISSN 0025-5564, 1990, vol. 101, no. 2, p. 155–235.
- [7] COLLI FRANZONE, P. - GUERRI, L. - ROVIDA, S. Wavefront propagation in an activation model of the anisotropic cardiac tissue: asymptotic analysis and numerical simulations. *J. Math. Biol.* ISSN 0303-6812, 1990, vol. 28, no. 2, p. 121–176.
- [8] MCFEE, R. - JOHNSTON, F. D. Electrocardiographic Leads I. Introduction. *Circulation.* ISSN 0009-7322, 1524-4539, 1953, vol. 8, no. 4, p. 554–568.
- [9] MACFARLANE, P. W. et al. *Basic Electrocardiology: Cardiac Electrophysiology, ECG Systems and Mathematical Modeling*. London : Springer, 2011. 497 p. ISBN 978-0-85729-870-6.
- [10] KIRK, D. B. - HWU, W. W. *Programming Massively Parallel Processors, Second Edition: A Hands-on Approach*. Amsterdam; Boston : Morgan Kaufmann, 2012. 514 p. ISBN 978-0-12-415992-1.

- [11] SCHMITT, O. H. Biological Information Processing Using the Concept of Interpenetrating Domains. *Inf. Process. Nerv. Syst.* Springer Berlin Heidelberg, 1969. ISBN: 978-3-662-23480-8, p. 325–331.
- [12] PULLAN, A. - CHENG, L. K. - BUIST, M. L. *Mathematically Modelling The Electrical Activity Of The Heart: From Cell To Body Surface And Back Again.* Wspc, 2005. 442 p.
- [13] COOK, S. *CUDA Programming: A Developer's Guide to Parallel Computing with GPUs.* Amsterdam ; Boston : Morgan Kaufmann, 2012. 600 p. ISBN 978-0-12-415933-4.
- [14] CHENG, J. - GROSSMAN, M. - MCKERCHER, T. *Professional CUDA C Programming.* Indianapolis, IN : Wrox, 2014. 528 p. ISBN 978-1-118-73932-7.
- [15] FARBER, R. *CUDA Application Design and Development.* Waltham, MA : Morgan Kaufmann, 2011. 336 p. ISBN 978-0-12-388426-8.
- [16] BOULAKIA, M. et al. Mathematical modeling of electrocardiograms: a numerical study. *Ann. Biomed. Eng.* ISSN 1573-9686, 2010, vol. 38, no. 3, p. 1071–1097.
- [17] TEN TUSSCHER, K. H. W. J. et al. A model for human ventricular tissue. *Am. J. Physiol. Heart Circ. Physiol.* ISSN 0363-6135, 2004, vol. 286, no. 4, p. H1573-1589.
- [18] TEN TUSSCHER, K. H. W. J. - PANFILOV, A. V. Cell model for efficient simulation of wave propagation in human ventricular tissue under normal and pathological conditions. *Phys. Med. Biol.* ISSN 0031-9155, 2006, vol. 51, no. 23, p. 6141–6156.
- [19] PRAVDIN, S. F. et al. Mathematical model of the anatomy and fibre orientation field of the left ventricle of the heart. *Biomed. Eng. Online.* ISSN 1475-925X, 2013, vol. 12, p. 54.
- [20] LEGRICE, I. J. et al. Laminar structure of the heart: ventricular myocyte arrangement and connective tissue architecture in the dog. *Am. J. Physiol.* ISSN 0002-9513, 1995, vol. 269, no. 2 Pt 2, p. H571-582.
- [21] YOUNG, R. J. - PANFILOV, A. V. Anisotropy of wave propagation in the heart can be modeled by a Riemannian electrophysiological metric. *Proc. Natl. Acad. Sci. U. S. A.* ISSN 1091-6490, 2010, vol. 107, no. 34, p. 15063–15068.
- [22] STREETER, D. D. Gross morphology and geometry of the heart. *Handb. Physiol.* 1979, vol. 1,
- [23] STREETER, D. D. et al. Fiber Orientation in the Canine Left Ventricle during Diastole and Systole. *Circ. Res.* ISSN 0009-7330, 1524-4571, 1969, vol. 24, no. 3, p. 339–347.
- [24] LEGRICE, I. J. - HUNTER, P. J. - SMAILL, B. H. Laminar structure of the heart: a mathematical model. *Am. J. Physiol.* ISSN 0002-9513, 1997, vol. 272, no. 5 Pt 2, p. H2466-2476.
- [25] ITÔ, K. *Encyclopedic Dictionary of Mathematics.* MIT Press, 2000.
- [26] BORNEMANN, F. - RASCH, C. Finite-element Discretization of Static Hamilton-Jacobi Equations based on a Local Variational Principle. *Comput. Vis. Sci.* ISSN 1432-9360, 1433-0369, 2006, vol. 9, no. 2, p. 57–69.
- [27] KIEFER, J. Sequential minimax search for a maximum. *Proc. Am. Math. Soc.* ISSN 0002-9939, 1088-6826, 1953, vol. 4, no. 3, p. 502–506.
- [28] WON-KI JEONG, R. T. W. A Fast Iterative Method for Eikonal Equations. *SIAM J Sci. Comput.* ISSN 1064-8275, 2008, vol. 30, no. 5, p. 2512–2534.
- [29] POTSE, M. - DUBÉ, B. - VINET, A. Cardiac anisotropy in boundary-element models for the electrocardiogram. *Med. Biol. Eng. Comput.* ISSN 0140-0118, 2009, vol. 47, no. 7, p. 719–729.
- [30] NGUYÊN, U. C. et al. An in-silico analysis of the effect of heart position and orientation on the ECG morphology and vectorcardiogram parameters in patients with heart failure and intraventricular conduction defects. *J. Electrocardiol.* ISSN 1532-8430, 2015, vol. 48, no. 4, p. 617–625.
- [31] COLLI FRANZONE, P. - PAVARINO, L. F. - SCACCHI, S. *Mathematical Cardiac Electrophysiology.* Cham : Springer International Publishing, vol. 13, 2014. ISBN 978-3-319-04800-0.
- [32] LORENSEN, W. E. - CLINE, H. E. Marching cubes: A high resolution 3D surface construction algorithm. *Comput. Graph.* 1987, vol. 21, no. 4, p. 163–169.
- [33] *The Digital Signal Processing Handbook, Second Edition - 3 Volume Set.* CRC Press, 2009. 2394 p. ISBN 978-1-4200-4563-5.
- [34] KALAVSKÝ, P. - TYŠLER, M. Real-time processing of multichannel ECG signals using graphic processing units. *Clinician and Technology.* 2012, vol. 42, no. 2, p. 27–30.
- [35] MUZIK, J. et al. *Procardio 8 – the 8th Generation of the High Resolution Ecg Mapping System.* 2009.
- [36] cuFFT. *NVIDIA Dev.* Accessible on: <<https://developer.nvidia.com/cufft>>.
- [37] Thrust - Parallel Algorithms Library. Accessible on: <<https://thrust.github.io/>>.

- [38] CSCS Home - Cscs. Accessible on: <<http://www.cscs.ch/index.html>>.
- [39] FU, Z. - KIRBY, R. - WHITAKER, R. A Fast Iterative Method for Solving the Eikonal Equation on Tetrahedral Domains. *SIAM J. Sci. Comput.* ISSN 1064-8275, 2013, vol. 35, no. 5, p. C473–C494.

### List of author's publications

- AED - KALAVSKÝ P., ROSÍK V., KARAS S., TYŠLER M. Measuring system with compound software architecture for measurement and evaluation of biosignals from isolated animal hearts. In MEASUREMENT 2011 : Proceedings of the 8th International Conference on Measurement - Bratislava : Institute of Measurement Science SAS, 2011, p. 379-382. ISBN 978-80-969-672-4-7.
- AEE - KALAVSKÝ P., ROSÍK V., KARAS S., TYŠLER M. Merací systém na merania a vyhodnocovanie biosignálov z izolovaných srdc malých zvierat. In Trendy v biomedicínskom inžinýrství 2011 : Sborník 9. česko-slovenské konference – Ostrava : VŠB - Technická univerzita Ostrava, 2011, s. 115-118, ISBN: 978-80-248-2479-6.
- ADE - KALAVSKÝ P., TYŠLER M. Real-time processing of multichannel ECG signals using graphic processing units. *Lékař a technika - Clinician and Technology*, 2012, vol. 42, no. 2, p. 27–30. ISSN 0301-5491.
- AED - TYŠLER M., ROSÍK V., KALAVSKÝ P., BUKOR G. Portable high resolution multichannel ECG measuring device. In Measurement 2013 : Proceedings of the 9th International Conference on Measurement – Bratislava : Institute of Measurement Science SAS, 2013, p. 161-164. ISBN 978-80-969-672-5-4.
- ADE - KALAVSKÝ P., TYŠLER M. Real-time visualization of multichannel ECG signals using a parallel programming approach. *Lékař a technika - Clinician and Technology*, 2014, vol. 44, no. 4, p. 5–9. ISSN 0301-5491.
- AFG - PEZZUTO S., KALAVSKY P., POTSE M., AURICCHIO A., KRAUSE R. Inverse modeling for cardiac electrophysiology with fast eikonal approximation. In: Fifth Chilean Workshop on Numerical Analysis of Partial Differential Equations. Concepción, January 2016.
- AFG - PEZZUTO S., KALAVSKY P., POTSE M., REGOLI F., CAPUTO M. L., CONTE G., MOCCHETTI T., AURICCHIO A. and KRAUSE R. Rapid estimation of 3D ventricular activation from electroanatomic mapping. In: *Cardiostim Europace*. Nice, June 2016.